Assimilation of NDVI data in a land surface – Vegetation model for leaf area index predictions in a tree-grass ecosystem

Nicola Montaldo, Andrea Gaspa & Roberto Corona

Published online: 19 Sep 2023.

Submit your article to this journal ⬀

View related articles ⬀

View Crossmark data ⬀

Assimilation of NDVI data in a land surface – Vegetation model for leaf area index predictions in a tree-grass ecosystem

Nicola Montaldo, Andrea Gaspa and Roberto Corona

Dipartimento di Ingegneria civile, ambientale e architettura, Università di Cagliari, Cagliari, Italy

ABSTRACT

Periodic observations of vegetation index, such as the normalized difference vegetation index (NDVI), can be used for data assimilation in heterogenous ecosystems. Indeed, the new Sentinel 2 Multispectral instrument and Landsat 8 Operational Land Imager sensor data are available at such high temporal and spatial resolutions that can be used to detect the patches of the main vegetation components (grass and trees) of heterogenous ecosystems, and capture their dynamics. We demonstrate the possibility to merge grass and tree NDVI observations and models, to optimally provide robust predictions of grass and tree leaf area index. The proposed assimilation approach assimilates NDVI data through the Ensemble Kalman filter (EnKF) and dynamically calibrates a key vegetation dynamic model parameter, the maintenance respiration coefficient (m_a). In the presence of large bias of the grass and tree m_a base values, only the use of the proposed assimilation approach removes the large bias in the biomass balance, dynamically calibrating maintenance respiration coefficients, and corrects the model. The performance of a land surface – vegetation model was improved by assimilating observations of NDVI. The effective impact of the proposed assimilation approach on the evapotranspiration and CO_2 uptake predictions in the heterogenous ecosystem is also demonstrated.

1. Introduction

The structure and function of the vegetation canopy regulates the exchange of mass, energy and momentum across the biosphere-atmosphere interface (Eagleson 2002; Lambers, Chapin III, and Pons 1998; Larcher 1995). Vegetation density controls the functioning of land surface processes through its impact on evapotranspiration, interception, and carbon uptake (Albertson and Kiely 2001; Arora 2002; Chen et al. 2015; Fatichi, Pappas, and Ivanov 2016; Fernandez-Illescas and Rodriguez-Iturbe 2004; Montaldo et al. 2003; Porporato and Rodriguez-Iturbe 2002; Rodriguez-Iturbe 2000).

The leaf area index (LAI) is a key vegetation characteristic, driver of the vegetation productivity, and can be considered a key biophysical variable in vegetation models (Ewert 2004; Parker 2020; Wythers, Reich, and Turner 2003). Indeed, efforts have led to improvements in the estimate of key ecohydrological variables, such as the LAI, from remote sensors (Houborg and McCabe 2018; McCabe et al. 2017; Pettorelli et al. 2014). LAI mapping can be derived from observations of optical remote sensors operating in the visible and infrared bands (Broge and Leblanc 2001; Fang et al. 2019; Zheng and Moskal 2009). Indeed, vegetation indexes, e.g. the normalized

difference vegetation index (NDVI), can be estimated from optical remote observations (Fang et al. 2019; Zheng and Moskal 2009), and NDVI is strictly related to LAI through empirical and physically-based models (Dong et al. 2019; Li et al. 2017; Verrelst et al. 2015; Wang et al. 2005). Nowadays, a wide variety of optical satellite remote sensors are available, at different spatial resolutions. They range, for instance, from the coarse spatial resolutions of AVHRR (1100 m) and MODIS (250-1000 m) to the fine spatial resolutions (10- 30 m) of ASTER, Landsat 8 and Sentinel 2 (Gim et al. 2020; Li et al. 2017; Ngadze et al. 2020), and the highest spatial resolutions (≤ 5 m) of IKONS, QUICKBIRD and WorldView (Huang et al. 2018). Originally, the main limit of optical sensors at high spatial resolution was the low time resolution of their platforms (Gao et al. 2006; Hill, Quaife, and Williams 2011), but new platforms, such as Sentinel 2 (Attarzadeh et al. 2018; Attarzadeh and Amini 2019) and Landsat 8 (Li et al. 2017; Ngadze et al. 2020), provide observations, potentially, at high temporal resolutions (up to 5–10 days), and are freely available. Observations of vegetation index at such high temporal resolutions are essential for operative data assimilation approaches, being vegetation phenology highly sensitive to temporal resolution (Jin et al. 2018; Kross et al. 2011; Thayn and Price 2008).

The fine spatial and time resolutions of the remote sensing data allow the vegetation mapping in heterogeneous ecosystems (Gao et al. 2006; Hill, Quaife, and Williams 2011), characterized by contrasting plant functional types (PFTs, e.g. grass and trees) competing for water and energy (Baldocchi, Xu, and Kiang 2004; Detto et al. 2006; Fernandez, Mora, and Novo 2004; Ramirez-Sanz et al. 2000; Scholes and Archer 1997; Williams and Albertson 2004). In these ecosystems, spatial patterns of tree and grass covers are variable in space and time, depending on the water availability and incoming radiation (Sankaran et al. 2005), both of which respond to topographic, climatic and edaphic factors, and ultimately produce the tree-grass mosaic on the landscape (Breshears 2006; Moore and Heilman 2011; Villegas et al. 2014). For capturing the fine spatial land cover variability and its evolution in time, remote optical sensing observations need to be at fine spatial and time resolutions (Hill, Quaife, and Williams 2011; Olsoy et al. 2017), which could be achieved, for instance, through the combined use of Landsat 8 and Sentinel 2 data. The fine spatial resolutions of Landsat 8 and Sentinel 2 allow to capture the patches of grass and trees in heterogeneous ecosystems.

Land surface models (LSMs) have been developed to simulate land and atmosphere interactions and the soil moisture and thermal states, from the integration of mass and energy balance equations (e. g., Albertson and Kiely 2001; Famiglietti and Wood 1994; Montaldo and Albertson 2001; Noilhan and Planton 1989; Wigmosta, Lettenmaier, and Vail 1994). LSMs have been coupled with vegetation dynamic models (VDM) for modeling vegetation dynamics and their interactions with land surface processes (Arora 2002; Montaldo et al. 2005; Montaldo, Albertson, and Mancini 2008). The coupled LSM-VDMs are part of the ecohydrological models, which are able to integrate hydrological mechanisms and ecological patterns and processes (Chen et al. 2015; Fatichi, Pappas, and Ivanov 2016; Rodriguez-Iturbe 2000). In a coupled LSM-VDM, vegetation characteristics such as the leaf area index (LAI), which were often considered to be yearly invariant or seasonally variable according to pre-defined shapes in LSMs (Arora 2002; Jasper et al. 2004; Vanrheenen et al. 2004), become variable and are predicted by the VDM (Montaldo et al. 2005; Montaldo, Albertson, and Mancini 2008).

Data assimilation techniques guide the ecohydrological models with observations of certain state variables from satellite remote sensors (Crow and Wood 2003; Fang et al. 2019; Montaldo et al. 2001; Montaldo, Albertson, and Mancini 2007; Reichle et al. 2004; Wigneron et al. 1999). Little effort has been made to assimilate LAI from optical remote sensing data in LSM (Bonan et al. 2020) and LSM coupled with a crop growth model or VDM (Cheng et al. 2020; Huang et al. 2015; Kumar et al. 2019; Migliavacca et al. 2009; Peng et al. 2021; Tripathy et al. 2013); most research mainly used remote observations at the coarse spatial scale of MODIS (Demarty et al. 2007; Fox et al. 2018; Li et al. 2017; Ma et al. 2017; Migliavacca et al. 2009; Quaife et al. 2008). MODIS observations do not seem suitable for highly heterogeneous, water-limited ecosystems due to the coarse spatial resolution (>250 m), which would not allow a clear distinction of

vegetation cover components (e.g. trees), which usually cover less than 50 m in these ecosystems. This study proposes the assimilation in the coupled LSM-VDM of observations from two optical satellites (Landsat 8 and Sentinel 2) with fine spatial and time resolutions, which could be appropriate for heterogeneous ecosystems.

Data assimilation accounts for both measurement and model errors optimally using, for instance, the Kalman filters (e.g. Reichle et al. 2002). The Kalman filter considers errors of the model from parameters, initial conditions and forcing (e.g. Dunne and Entekhabi 2005; Margulis et al. 2002; Montaldo, Albertson, and Mancini 2007). The Kalman filter should optimally assimilates measurements of state variables, such as provided by remote sensor data (e.g. soil moisture, leaf area index, surface temperature), to reduce the model errors. Besides Kalman filters, other data assimilation algorithms are variational assimilations (Jin et al. 2018), which assimilates all observations at once at their respective measurement times over a given period (Scholze et al. 2017), in contrast with the sequential assimilation approach used by Kalman filters and Particle filters, which assimilates observations subsequently at discrete model time steps (Jin et al. 2018). Reichle et al. (2002) suggested the use of the ensemble Kalman filter (EnKF) of Evensen (1994), because it is '*more robust and offers more flexibility in covariance modeling*'. The EnKF is widely used in land data assimilation and hydrology (Crow 2003; Crow and Wood 2003; Evensen 2003; Margulis et al. 2002; Montaldo, Albertson, and Mancini 2007; Reichle et al. 2002; Reichle et al. 2019) due to its relative ease of implementation (Reichle et al. 2017). Some data assimilation efforts assimilated NDVI and LAI data in ecohydrological models using EnKF (Dong et al. 2013; Fox et al. 2018; Kumar et al. 2019; Li et al. 2017; Ling et al. 2019; Ma et al. 2017; Quaife et al. 2008). The Kalman filter assumes that the model errors are zero-mean and uncorrelated in time. In ecohydrologic modeling this requirement is frequently not respected, and the model becomes biased. Montaldo, Albertson, and Mancini (2007) assimilated soil moisture observations in a LSM using EnKF and developed an assimilation approach that dynamically calibrated a key soil water balance model parameter as a function of the persistent bias in soil moisture predictions. This approach was useful when model parameters largely differed from the calibrated values (Montaldo, Albertson, and Mancini 2007), and was applied using Sentinel 1 radar data by Montaldo et al. (2022). Lü et al. (2011a, 2011b) followed the approach of Montaldo, Albertson, and Mancini (2007) assimilating soil moisture in two Chinese field sites, and Nie, Zhu, and Luo (2011) and Zhang et al. (2017) assimilating soil moisture using EnKF, and calibrated several parameters of a soil water balance model, by using field measurements and not using remote sensor observations.

Here, the performance of the EnKF for LAI predictions is addressed for reducing LSM-VDM biases due to parameter errors. Using the Montaldo, Albertson, and Mancini (2008) coupled LSM-VDM, we propose an approach for assimilating tree and grass NDVI from Landsat 8 and Sentinel 2 remote sensors in the LSM-VDM, which removes the model biases through a dynamic calibration of key VDM parameters.

The proposed multiscale assimilation approach was tested in a Sardinian field site, characterized by strong heterogeneity with wild olives randomly distributed in surrounding grass, and water-limited conditions typical of Mediterranean ecosystems (Detto et al. 2006). In the Sardinian field site, a micrometeorological eddy-covariance based tower has been operating (Montaldo, Albertson, and Mancini 2008; 2020), and Landsat 8 and Sentinel 2 remote observations were used for data assimilation. Analogous solutions should be derivable for most other ecohydrological models, and using data of other remote sensors with similar or higher spatial and temporal resolutions. In summary, our objectives are to:

1) assimilate tree and grass NDVI observations of optical satellites at fine spatial resolution (Landsat 8 and Sentinel 2) in a coupled LSM-VDM over an heterogenous ecosystem;
2) dynamically calibrate key VDM parameters for LAI predictions, through a proposed approach based on the manipulation of the conservation equations of green and tree biomass; and
3) evaluate the effectiveness of the proposed assimilation approach for predictions of key land surface fluxes, such as evapotranspiration and CO_2 assimilation.

2. Methods

In this section we describe the proposed approach for assimilating NDVI data in a coupled LSM-VDM. The case study and data are then presented.

2.1. The assimilation approach

The proposed multiscale assimilation approach includes (Figure 1): 1) the LSM running at a fine time scale (e.g. half hourly), 2) the VDM that predicts LAI dynamics at a coarser time scale of (e.g. daily), 3) the NDVI observations from remote sensors at a larger time scale (e.g. weekly), which are assimilated through the EnKF, 4) the updating of model parameters at a further larger time scale (e.g. three weeks or more).

Below, each component of the proposed assimilation approach is described.

2.1.1. The coupled LSM-VDM

The ecohydrological model is a three-component coupled land surface – vegetation dynamic model. The VDM estimates the LAI evolution through time for two vegetation components (grass and trees), which are used by the LSM for computations of the energy exchanges between soil and vegetation (Figure 2). The details are given in Montaldo, Albertson, and Mancini (2008). Here, a summary of the main components are described.

2.1.1.1. The land surface model. The LSM predicts the dynamics of water and energy fluxes at the land surface on a half-hour time step (Figure 1). It includes three components of land surface: bare soil, grass and trees. The root zone supplies the bare soil and vegetation with soil moisture for evapotranspiration and controls the infiltration and runoff mechanisms. Equations for surface temperature and the components of the energy balance are applied separately for each land cover component, so that the model predicts the energy balance distinctly for each land cover component (Montaldo, Albertson, and Mancini 2008) (Table 1).

The soil water balance equation of the root zone is computed by

$$\frac{\partial \theta_{rz}}{\partial t} = \frac{1}{d_{rz}}(f_{bs}I_{bs} + f_{v,t}I_t + f_{v,g}I_g - f_{bs}E_{bs} - f_{v,t}E_t - f_{v,g}E_g - q_D) \tag{1}$$

where θ_{rz} is the soil moisture of the root zone, d_{rz} is the root zone depth, I_{bs} is the infiltration rate on bare soil, I_t and I_{gr} are the throughfall rates infiltrating into the soil covered by trees and grass respectively, q_D
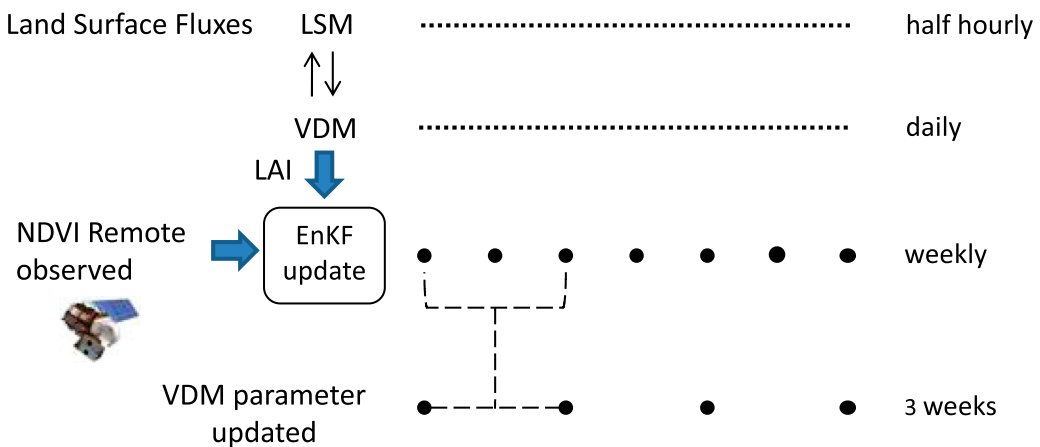

Figure 1. The multiscale assimilation scheme. LSM is the land surface model, VDM is the vegetation dynamic model, EnKF is the ensemble Kalman filter, and LAI is the leaf area index. On the right is an example of the time scale of each component of the assimilation scheme.
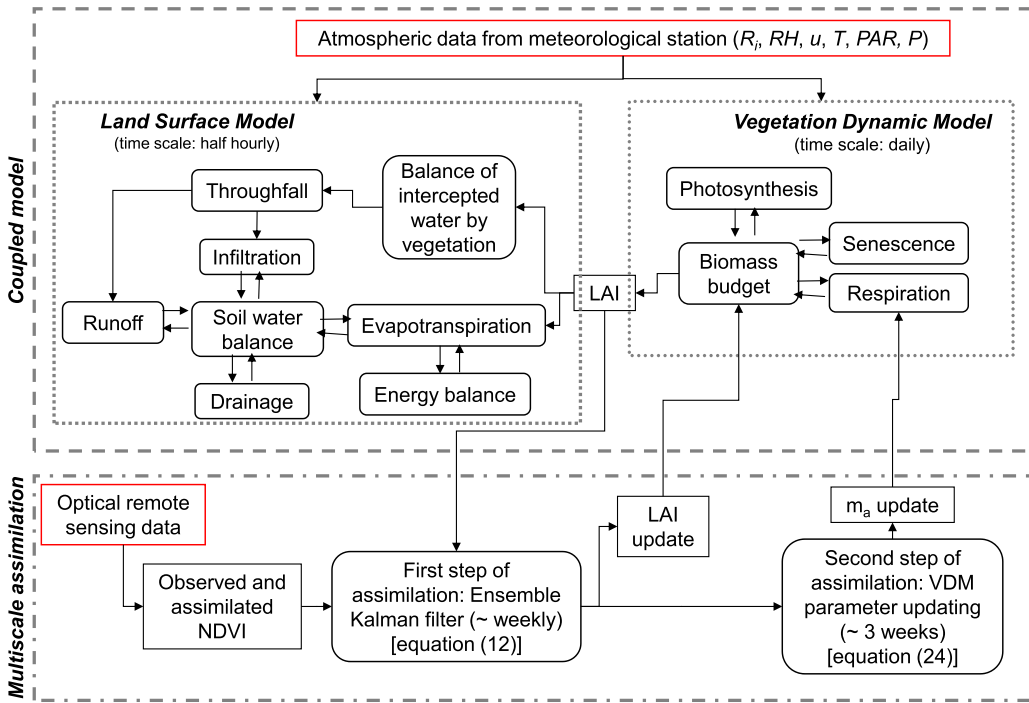
Figure 2. The technical workflow (flowchart) of the assimilation approach.

is the rate of drainage out of the bottom of the root zone, E_{bs} is the rate of bare soil evaporation, E_t and E_g are the rates of transpiration of trees and grass respectively, $f_{v,t}$ is the fraction of tree cover, $f_{v,g}$ is the fraction of grass cover, and f_{bs} is the fraction of bare soil (Montaldo, Albertson, and Mancini 2008). The throughfall rate is modeled through a balance equation of the intercepted water by the canopy reservoir, which storage capacity is a function of the LAI (= 0.2 LAI; Noilhan and Planton 1989) and produces throughfall when the reservoir is saturated (Montaldo and Albertson 2001; Noilhan and Planton 1989). An infiltration excess mechanism, based on the Philip's infiltration equation (Philip 1957), is used for the infiltration. The q_D rate is estimated using the unit head gradient assumption (Table 1; Albertson and Kiely 2001; Montaldo, Albertson, and Mancini 2008).

E_t and E_g are estimated distinctly using the Penman-Monteith equation (e.g. Brutsaert 1982, 224) for each vegetation component, with canopy resistances estimated using a typical Jarvis (1976) approach (Table 1). The actual rate of bare soil evaporation is determined as $\alpha(\theta)PE$, where $\alpha(\theta)$ is a rate-limiting function, and PE is the potential evaporation estimated by the Penman equation (e.g. Brutsaert 1982, equations 10.15, 10.16 and 10.19). Hence, the total evapotranspiration is estimated as:

$$ET = f_{bs}E_{bs} + f_{v,t}E_t + f_{v,g}E_g \tag{2}$$

Paralleling the approach for ET estimation, a 3-component approach is implemented for estimating the total net CO_2 flux (Montaldo, Corona, and Albertson 2013):

$$F_c = f_{v,t}F_{c,t} + f_{v,g}F_{c,g} + R_{bs} \tag{3}$$

where $F_{c,t}$ and $F_{c,g}$ are the carbon exchange of trees and grass, respectively, and R_{bs} is the soil respiration. Carbon exchange rates for each PFT (i.e. $F_{c,t}$, $F_{c,g}$) are computed as the difference between photosynthesis and growth respiration (Table 2). Soil respiration is estimated as a function of the temperature (Table 2; Montaldo, Corona, and Albertson 2013; Novick et al. 2004; Ruehr and Buchmann 2010). The model parameters are presented in Table 3.

Table 1. Equations of drainage (q_D), canopy resistance (r_c) with stress functions of soil moisture (θ), air temperature (T_a) and vapor pressure deficit (VPD), sensible heat flux (H), net radiation (R_n), soil heat flux (G), and surface temperature (T_s) in the LSM. Parameters are defined in Table 3.

Equations

Drainage

$$q_D = k_s \left(\frac{\theta}{\theta_s}\right)^{2b+3}$$

Canopy resistance

$$r_c = \frac{r_{s,min}}{LAI[f_1(\theta)f_2(T_a)f_3(VPD)]^{-1}}$$

$$f_1(\theta) = \begin{cases} 0 & \text{if } \theta \leq \theta_{wp} \\ \dfrac{\theta - \theta_{wp}}{\theta_{lim} - \theta_{wp}} & \text{if } \theta_{wp} < \theta < \theta_{lim} \\ 1 & \text{if } \theta \geq \theta_{lim} \end{cases}$$

$$f_2(T_a) = \begin{cases} 0 & \text{for } T_a \leq T_{a,min} \text{ and } T_a > T_{a,max} \\ 1 - \dfrac{T_{a,opt} - T_a}{T_{a,opt} - T_{a,min}} & \text{for } T_{a,min} < T_a < T_{a,opt} \\ 1 & \text{for } T_{a,opt} \leq T_a \leq T_{a,max} \end{cases}$$

$$f_3 = 1 - \omega \log(VPD)$$

Sensible heat flux

$$H = \rho_a c_p C_H u(T_s - T_a),$$

where C_H the heat transfer coefficient

Net radiation

$$R_n = R_{swin}(1 - \alpha) + \varepsilon(R_{lwin} - \sigma T_s^4),$$

with shortwave incoming ration, R_{swin}, longwave incoming ration, R_{lwin}, estimated based on equation 6.10 in Brutsaert (1982), a albedo, ε emissivity and σ the Stefan-Boltzmann constant

Soil heat flux

$$G = R_n\text{-}H\text{-}LE$$

Surface temperature

$$\frac{dT_s}{dt} = C_T G - \frac{2\pi}{\tau}(T_s - T_a),$$

with T_2 being the mean T_s value over one day τ, and C_T the soil thermal coefficient

$$\frac{dT_2}{dt} = \frac{1}{\tau}(T_s - T_2)$$

2.1.1.2. The vegetation dynamic model. The VDM computes the change in biomass over time from the difference between the rates of biomass production (photosynthesis) and loss, mainly through respiration (e.g. Cayrol et al. 2000; Larcher 1995). The VDM distinguishes tree and grass components. In the VDM of trees, four separate biomass states are considered: green leaves (B_l), stem (B_s), living root (B_r), and standing dead (B_d). However, the VDM of grass only distinguishes three biomass states (green leaves, roots and standing dead). The biomass [g DM m^{-2}] components are simulated through ordinary differential equations, integrated numerically at a daily time step (Montaldo, Albertson, and Mancini 2008):

$$\frac{dB_l}{dt} = a_a Ph - R_{l,\mu} - R_{l,\gamma} - S_l \tag{4}$$

$$\frac{dB_s}{dt} = a_s Ph - R_{s,\mu} - R_{s,\gamma} - S_s \tag{5}$$

Table 2. Equations of the vegetation dynamic model components. Parameters are defined in Table 3.

Ecophysiological term	Equations
Photosynthesis	$Ph = \varepsilon_P(PAR) f_{PAR} PAR \dfrac{1.37 r_a + 1.6 r_{c,min}}{1.37 r_a + 1.6 r_c}$ $\varepsilon_P(PAR) = a_0 + a_1 PAR + a_2 PAR^2$ $f_{PAR} = 1 - e^{-k_e LAI}$
Allocation	For the tree cover: $a_a = \dfrac{\xi_a}{1 + \Omega[2 - \lambda - f_1(\theta)]}$ $a_s = \dfrac{\xi_s + \Omega(1 - \lambda)}{1 + \Omega[2 - \lambda - f_1(\theta)]}$ $a_r = \dfrac{\xi_r + \Omega(1 - f_1(\theta))}{1 + \Omega[2 - \lambda - f_1(\theta)]}$ $\xi_a + \xi_s + \xi_r = 1; \; \lambda = e^{-k_e LAI}$

For grass cover:

$$a_a = \frac{\xi_a + \Omega\lambda}{1 + \Omega[1 + \lambda - f_1(\theta)]}$$

:

$$a_r = \frac{\xi_r + \Omega(1 - f_1(\theta))}{1 + \Omega[1 + \lambda - f_1(\theta)]}$$

$$\xi_a + \xi_r = 1$$

Respiration	Maintenance and growth respirations of biomass components

$$R_{l,\mu} = m_a f_4(T) B_l; \; R_{l,\gamma} = g_a a_a P_g$$

$$R_{s,\mu} = m_s f_4(T) B_s; \; R_{s,\gamma} = g_s a_s P_g R_{r,\mu} = m_r f_4(T) B_r; \; R_{r,\gamma} = g_r a_r P_g$$

$f_4(T) = Q_{10}^{\frac{T_m}{10}}$ with T_m = mean daily temperature

Soil respiration

$$R_{bs} = R_{10} Q_N^{\frac{T_m}{10}}$$

where R_{10} is the reference respiration rate at 10°C and Q_N is the soil respiration sensitivity to temperature.

Senescence	$S_l = d_a B_l$ $S_s = d_s B_s$ $S_r = d_r B_r$
Litterfall	$L_a = k_a B_d$

$$\frac{dB_r}{dt} = a_r Ph - R_{r,\mu} - R_{r,\gamma} - S_r \tag{6}$$

$$\frac{dB_d}{dt} = S_l - L_a \tag{7}$$

where Ph is the gross photosynthesis, a_a, a_s and a_r are allocation (partitioning) coefficients to leaves, stem and root states, $R_{l,\mu}$, $R_{s,\mu}$ and $R_{r,\mu}$ are the maintenance respiration rates from leaves, stem and root biomass respectively, $R_{l,\gamma}$, $R_{s,\gamma}$ and $R_{r,\gamma}$ are the growth respiration rates from leaves, stem and root biomass respectively, while S_g, S_s and S_r are the senescence rates of leaves, stem and root

Table 3. Model parameters of the coupled LSM-VDM and their values for the Orroli site.

Parameter	Description	Value* grass	Value* tree
LSM-VDM parameters			
$r_{s,min}$ [s m^{-1}]	minimum stomatal resistance	100	300
T_{min} [°K]	minimum temperature	272.15	272.15
T_{opt} [°K]	optimal temperature	295.15	285.15
T_{max} [°K]	maximum temperature	313.15	318.15
θ_{wp} [−]	wilting point	0.08	0.04
$\theta_{lim,}$ [−]	limiting soil moisture for vegetation	0.20	0.17
ω [KPa^{-1}]	slope of the f_3 relation	0.6	0.6
Only VDM parameters			
c_l [m^2 gDM^{-1}]	Specific leaf areas of the green biomass in growing season	0.01	0.005
c_d [m^2 gDM^{-1}]	Specific leaf areas of the dead biomass	0.01	0.003
k_e [−]	PAR extinction coefficient	0.5	0.5
ξ_a [−]	Parameter controlling allocation to leaves	0.6	0.55
ξ_s [−]	Parameter controlling allocation to stem	−	0.1
ξ_r [−]	Parameter controlling allocation to roots	0.4	0.35
Ω [−]	Allocation parameter	0.8	0.8
m_a [d^{-1}]	Maintenance respiration coefficients for aboveground biomass	0.032	0.001
g_a [−]	Growth respiration coefficients for aboveground biomass	0.28	0.69
m_r [d^{-1}]	maintenance respiration coefficients for root biomass	0.007	0.002
g_r [−]	growth respiration coefficients for root biomass	0.1	0.1
Q_{10} [−]	Temperature coefficient in the respiration process	2.45	2.42
d_a [d^{-1}]	death rate of aboveground biomass	0.05	0.0045
d_r [d^{-1}]	death rate of root biomass	0.003	0.005
k_a [d^{-1}]	rate of standing biomass pushed down	0.05	0.35
Only LSM parameters			
$z_{om,v}$ [m]	Vegetation momentum roughness length	0.05	0.5
$z_{ov,v}$ [m]	Vegetation water vapor roughness length	z_{om}/7.4	z_{om}/2.5
$z_{om,bs}$ [m]	Bare soil momentum roughness length	0.015	
$z_{ov,bs}$ [m]	Bare soil water vapor roughness length	z_{om}/10	
θ_s [−]	saturated soil moisture	0.53	
b [−]	slope of the retention curve	8	
k_s [m/s]	saturated hydraulic conductivity	5×10^{-6}	
$|\psi_s|$ [m]	air entry suction head	0.79	
d_{rz} [m]	Root zone depth	0.19	

*Two values for vegetation parameters are those of the grass and tree.

biomass, respectively, and L_a is the litter fall. The model equations are given in Table 2 and the parameters are presented in Table 3, where calibrated values are reported.

The leaf area index is estimated from the biomass by a linear relationship (Arora 2003; Hanson, Skiles, and Parton 1988; Montaldo et al. 2005; Nouvellon et al. 2000):

$$LAI = c_l \, B_l \tag{8}$$

where c_l is the specific leaf area of the green biomass, which is different for grass and trees (Table 3). In the case of LAI predictions of grass, the Equation (5) is not used because the VDM of grass only distinguishes three biomass states (green leaves, roots and standing dead) and not stem biomass. The VDM provides estimates of daily values of leaf biomass and, thus, the LAI of the tree and grass, which is used by the LSM to estimate evapotranspiration, energy flux, rainfall interception, carbon assimilation, and the soil water content at a half-hour time step (Figure 2; Montaldo, Albertson, and Mancini 2008). The LSM provides soil moisture and aerodynamic resistances to the VDM (Figure 2). The details are given in Montaldo et al. (2005), Montaldo, Albertson, and Mancini (2008), and Montaldo, Corona, and Albertson (2013).

2.1.2. Optical remote sensing data

NDVI is estimated from red and near-infrared spectral reflectance measurements of satellite remote sensors (Figure 2). The Operational Land Imager (OLI) – Landsat 8 data is mainly used, and, secondly, the Sentinel 2 Multi Spectral Imager (MSI) data increases the optical database. Landsat 8 has

a temporal resolution of 8-days and a spatial resolution of 30 m for the optical bands (panchromatic band at 15 m spatial resolution), which is similar to Sentinel 2 data, and both are freely available.

From Landsat 8 and Sentinel 2 observations, NDVI is estimated at 30 m spatial resolution for being assimilated in the EnKF based approach. LAI is related to NDVI through the Γ operator using an empirical approach (e.g. Gupta, Prasad, and Vijayan 2000; Potithep et al. 2010; Wang et al. 2005):

$$LAI = \Gamma(NDVI) = \beta_1 + \beta_2 NDVI^{\beta_3} \qquad (9)$$

where β_1, β_2 and β_3 are coefficients for vegetation species. The values of β_1, β_2 and β_3 have been estimated for the case study from simultaneous observations of LAI in the field and NDVI from remote sensors. Note that analogous solutions should be derivable with different $\Gamma(NDVI)$ relationships.

2.1.3. The ensemble Kalman filter

We assimilate observations of NDVI, which is related to LAI through (9), in the VDM, which describes the evolution of LAI. In the Kalman filters, $\vec{\varphi}$ is a vector of surface state variables (in this case LAI). The equation describing the evolution of $\vec{\varphi}$ (at the t_i time step), as determined by a nonlinear model ($\vec{f}$, in this case the vegetation dynamic model) can be written as (e.g. Crow and Wood 2003):

$$\frac{d\vec{\varphi}}{dt} = \vec{f}(\vec{\varphi}, \vec{\omega}) \qquad (10)$$

where $\vec{\omega}$ relates errors in model physics, parameterization, and/or forcing data, and is taken to be with mean zero and covariance $\vec{\Omega}$. $\vec{H}$ is the operator that represents the observation process which relates $\vec{\varphi}$ to the actual measurements available at time t_j (with $j = N_{la}$, 2, 3 N_{la}, … N, and N_{la} the number of Δt_1 model time steps in Δt_2 measurement time steps)

$$\vec{\delta}(t_j) = \vec{H}[\vec{\varphi}(t_j)] + \vec{\varepsilon}(t_j) \qquad (11)$$

where $\vec{\varepsilon}$ represents the vector of measurement errors, assuming a probabilistic distribution with zero mean and covariance $\vec{R}$.

In the EnKF (Evensen 1994; Reichle et al. 2002), an ensemble of φ^ζ ($\zeta = 1, \ldots, N_e$, with N_e the size of the ensemble) is predicted in parallel, using (10). The EnKF updates each ensemble member separately, using the $\vec{\delta}(t_j)$ observation and the diagnosed state error covariance $\overrightarrow{P^-}(t_j)$ (e.g. Reichle et al. 2002, Equation 6b). The superscripts '–' and '+' refer to the state estimates before and after the update at time t_j, respectively. Ensemble members are updated using (Reichle et al. 2002):

$$\overrightarrow{\varphi^{\zeta+}} = \overrightarrow{\varphi^{\zeta-}} + \vec{K}[\vec{\delta} - \vec{H}(\overrightarrow{\varphi^{\zeta-}}) + \overrightarrow{\varepsilon^\zeta}] \qquad (12)$$

where $\vec{K}$ is the Kalman gain, which depends on $\overrightarrow{P^-}$, and $\overrightarrow{\varepsilon^\zeta}$ is a random realization of the measurement error, which should have the same statistical properties as the error included in (11) (Margulis et al. 2002). The mean of the ensemble members, $\bar{\varphi}^+(t_j)$ is the state estimate of the variables.

Model errors in the EnKF are included through errors in the VDM initial conditions, physical parameters and forcing data. Errors of i) LAI initial conditions, ii) incoming short-wave solar radiation (R_{swin}), and the Photosynthetically Active Radiation (PAR), and iii) model parameters, such as the maintenance respiration coefficients for aboveground biomass (m_a) of grass and trees (Table 2), are included. We chose m_a as the VDM parameter for data assimilation after a sensitivity analysis of LAI to VDM parameters, which proved the high sensitivity of grass and tree LAI to m_a. Indeed, we performed an univariate sensitivity analysis of LAI to VDM parameters for tree and grass (m_a, g_a, Q_{10}, ξ_a, Ω, $r_{s,min}$, θ_{lim}, θ_{wp}), varying parameter values in a range of ±50% of the calibrated values

(which are in Table 3). When we varied the m_a parameter we found the largest effects on predictions of both grass (from 72% to 224% of the calibrated mean LAI value) and tree (from 14% to 121% of the calibrated mean LAI value) LAI, while varying the other parameters the variations of LAI predictions were less than half.

The ensemble of LAI initial values was generated by altering a particular value of LAI through the addition of a normally distributed perturbation with mean zero and SD_{LAI} standard deviation. At each time step, the ensembles of R_{swin} and PAR were generated by multiplying the recorded R_{swin} and PAR values by normally distributed random variables. The ensembles of grass and trees maintenance respiration coefficients ($m_{a,g}^\zeta$ for grass and $m_{a,t}^\zeta$ for trees), were generated as being normally distributed with means of $\hat{m}_{a,g}$ and $\hat{m}_{a,t}$ and standard deviations of SD_{mag} and SD_{mat}, respectively.

In this way, ensembles of LAI^ζ of grass and trees, which include model errors, were generated and evolved in time according to (4) and (8). The $\vec{\delta}(t_j)$ observations were obtained including the $\overrightarrow{NDVI^\zeta}$ random error in the NDVI observations derived from Landsat 8 (or Sentinel 2) according to (11), where the operator $\vec{H}$ is the inverse of Γ in (9). When observations from Landsat 8 (or Sentinel 2) are available, the ensemble of LAI^ζ (i.e. $LAI^{\zeta-}(t_j)$) is replaced by (or updated to) the ensemble $LAI^{\zeta+}(t_j)$, which is optimally estimated by (12) using the $\vec{\delta}(t_j)$ observations. Again, the state estimates of grass and tree LAI are given by the means of the ensembles. Hence, the EnKF filters the errors in observations of NDVI, which is related to LAI through (9), and the errors in LAI predictions made by the VDM.

2.1.4. The proposed approach for the parameter updating

The EnKF approach compensates for both inaccurate initial conditions and moderate model parameter errors. Here, we propose a method for adjusting a VDM parameter, the maintenance respiration coefficient for above-ground biomass, over a longer time scale than the remote sensing observation time scale when it largely diverges from calibrated values (Table 3). The proposed method updates (i.e. dynamically adjusts) m_a based on observations of persistent bias in the modeled biomass (i.e. LAI). The proposed procedure derives the required m_a adjustment from the conservation equation of the biomass (i.e. LAI) and is the same for grass and tree LAI. Substituting (8) in (4), the biomass balance for the modeled 'm' state variables is:

$$\frac{1}{c_l}\frac{\partial LAI^m}{\partial t} = a_a Ph^m - R_{l,\mu}^m - R_{l,\gamma}^m - S_l^m \tag{13}$$

Since the biomass balance must be conserved in both the model and reality, we write (13) for observed 'o' state variables.

$$\frac{1}{c_l}\frac{\partial LAI^o}{\partial t} = a_a Ph^o - R_{l,\mu}^o - R_{l,\gamma}^o - S_l^o \tag{14}$$

Assuming that $Ph^m \equiv Ph^o$, $R_{l,\gamma}^m \equiv R_{l,\gamma}^o$, and $S_l^m \equiv S_l^o$, and subtracting (14) from (13),

$$\frac{1}{c_l}\left(\frac{\partial LAI^o}{\partial t} - \frac{\partial LAI^m}{\partial t}\right) = \frac{1}{c_l}\frac{\partial(\Delta LAI^{o,m})}{\partial t} = R_{l,\mu}^m - R_{l,\mu}^o \tag{15}$$

where $\Delta LAI^{o,m}$ is the assimilation correction. From the maintenance respiration equation (Table 2) and (8):

$$R_{l,\mu}^m = R_{l,\mu}(LAI^m) = m_a^m f_3(T)^m B_l^m = m_a^m \frac{f_3(T)^m}{c_l} LAI^m \tag{16}$$

$$R_{l,\mu}^o = R_{l,\mu}(LAI^o) = m_a^o \frac{f_3(T)^o}{c_l} LAI^o \tag{17}$$

assuming that $f_3^m(T) \equiv f_3^o(T)$, the first-order Taylor series expansion of the maintenance respiration function about the modeled parameter values relates the modeled maintenance respiration to the 'real' maintenance respiration, in terms of differences between modeled and 'real' LAI and maintenance coefficient values

$$R_{l,\mu}(LAI^o, m_a^o) = R_{l,\mu}(LAI^m, m_a^m) + \frac{\partial R_{l,\mu}}{\partial m_a} \Delta m_a^{o,m} + \frac{\partial R_{l,\mu}}{\partial LAI} \Delta LAI^{o,m} \tag{18}$$

where

$$\Delta m_a^{o,m} = m_a^o - m_a^m \tag{19}$$

Substituting (18) into (15) relates the difference between 'real' and modeled LAI to the difference between 'real' and modeled maintenance coefficient values

$$\frac{\partial (\Delta LAI^{o,m})}{\partial t} = -c_l \left(\frac{\partial R_{l,\mu}}{\partial m_a} \Delta m_a^{o,m} + \frac{\partial R_{l,\mu}}{\partial LAI} \Delta LAI^{o,m} \right) \tag{20}$$

Differentiating (16) and substituting into (20) yields

$$\frac{\partial (\Delta LAI^{o,m})}{\partial t} = -c_l \left[\frac{f_3(T)}{c_l} LAI^m \Delta m_a^{o,m} - \frac{f_3(T)}{c_l} m_a^m \Delta LAI^{o,m} \right] \tag{21}$$

Solving (21) for the 'real' maintenance respiration coefficient, in terms of known quantities

$$m_a^o = m_a^m - \frac{m_a^m}{LAI^m} \Delta LAI^{o,m} - \frac{1}{f_3(T)LAI^m} \frac{\partial (\Delta LAI^{o,m})}{\partial t} \tag{22}$$

This expression would, theoretically, provide an estimate of the actual m_a at each time the LAI is updated through NDVI, from knowledge of the change in $\Delta LAI^{o,m}$ since the last update. However model parameter updating over a short interval is ill advised (Montaldo and Albertson 2003; Montaldo, Albertson, and Mancini 2007), as instantaneous measurement errors would induce detrimental shocks in the model. We propose updating over a reasonable averaging period, to relate persistent bias (as defined by a time average) to model parameter bias. By averaging (22) over an appropriate time interval (Δt_3, e.g. 3 weeks, Figure 1) to capture a reliable estimate of the 'persistent' LAI bias, we are able to estimate the required change in the maintenance respiration coefficient needed to reduce the model bias

$$m_a^o = m_a^m - \overline{\frac{m_a^m}{LAI^m} \Delta LAI^{o,m}} - \overline{\frac{1}{f_3(T)LAI^m} \frac{\partial (\Delta LAI^{o,m})}{\partial t}} \tag{23}$$

where we employ the overbar to denote a time averaged term. From inspection of (23), it is apparent that the process of averaging the LAI increments derived from the state variable assimilation will cancel temporally uncorrelated noise in favor of retaining the long-term persistent bias. When (23) is used in the EnKF, we need to update each component of the $m_{a,g}^\zeta$ and $m_{a,t}^\zeta$ ensembles over the Δt_3 time interval, which coincides with time steps t_k ($k = N_{la}N_{ma}, 2N_{la}N_{ma}, \dots N$ and

N_{ma} the number of Δt_2 steps in Δt_3, i.e. $\Delta t_3 = N_{ma} \Delta t_2 = N_{la} N_{ma} \Delta t_1$), through

$$m_a^{\zeta+}(t_k) = m_a^{\zeta-}(t_k) - \xi_1 - \xi_2 \tag{24}$$

$$\xi_1 = \frac{1}{N_{ma}} \sum_{j=k-(N_{ma}N_{la})+N_{la}}^{k,by\ N_{la}} \left[\frac{m_a^{\zeta-}(t_k)}{LAI^{\zeta-}(t_j)} (LAI^{\zeta+}(t_j) - LAI^{\zeta-}(t_j)) \right] \tag{25}$$

$$\xi_2 = \frac{1}{N_{ma}} \sum_{j=k-(N_{ma}N_{la})+N_{la}}^{k,by\ N_{la}} \frac{[LAI^{\zeta+}(t_j) - LAI^{\zeta-}(t_j)] - [LAI^{\zeta+}(t_{j-N_{la}}) - LAI^{\zeta-}(t_{j-N_{la}})]}{f_3(t_j)LAI^{\zeta-}(t_j)\Delta t_2} \tag{26}$$

where the notation in the summation operator gives an averaging from $(k - N_{ma}N_{la} + N_{la})$ to k in increments of N_{la}. In this way, an estimate of the 'persistent' LAI bias is used for evaluating the necessary change in the m_a. Thereby, after a learning (calibration) period the error of the model can be eliminated, allowing to restore a main assumption of the Kalman filter, which is zero mean model error. The solution is the same for grass ($m_{a,g}^{\zeta+}$) and tree ($m_{a,t}^{\zeta+}$) maintenance respiration coefficients.

In short, the multiscale assimilation scheme includes (Figures 1 and 2):

1) the land surface model, which run at the half hourly time scale, required for predicting the diurnal dynamics of water and energy balance terms;
2) the VDM-predicted LAI dynamics of grass and trees through (4) and (8) at a daily time scale, generating the ensembles of LAI at the t_i time intervals;
3) the EnKF, which filters the NDVI remote data (9) of grass and trees, available over the t_j time intervals (e.g. weekly) with model errors and measurements, and optimally updates the ensembles of $LAI^{\zeta-}(t_j)$ of grass and trees through (12) to arrive at $LAI^{\zeta+}(t_j)$;
4) the updating of the m_a^{ζ} ensembles of grass and trees through (24) over the t_k time intervals (e.g. 3 weeks).

Hereafter, we indicate the ensemble open loop without assimilation (i.e. only steps 1-2) as 'EnOL', with 'EnKF' being the assimilation approach that includes the ensemble Kalman filter only (i.e. step 1-3), and with 'EnKFdc' being the assimilation approach that includes the four steps described above.

Because the performance of the assimilation approach has to be proven for increasing uncertainty of the model (given the observation errors), the proposed assimilation approach will be tested for increasing errors in grass and tree m_a model parameters, comparing EnOL, EnKF, and EnKFdc performance.

2.2. Case study

The proposed assimilation approach was tested with observations from a field site at Orroli, Italy, located in east-central Sardinia (39°41'12.57" N, 9°16'30.34" E, 500 m a.s.l.; Detto et al. 2006; Montaldo, Albertson, and Mancini 2008; Montaldo, Corona, and Albertson 2013; Montaldo et al. 2020). The landscape is a patchy mixture of woody vegetation, where the dominant tree species is wild olive with a variable height of 3.5–4.5 m (∼33% of the footprint area), and herbaceous and grass species, on a gently sloping plateau (∼3° from NW to SE). The grass species grow during wet seasons and reach approximate heights of 0.5 m in spring. The soil thickness varies from 15 to 40 cm, averaging 17 cm ± 6 cm (standard deviation, SD) above a fractured basalt (Montaldo, Albertson, and Mancini 2008; Montaldo, Corona, and Albertson 2013). The climate at the flux site is maritime Mediterranean, with a mean annual precipitation of 643 mm, and mean July precipitation of 11 mm. Mean annual air temperature (T_a) is 14.6 °C, with mean July T_a of 23.7 °C.

2.2.1. Field data

A 10 m micrometeorological station was operating at the site to measure land-atmosphere flux of energy, water and carbon in addition to key state variables. The apparatus included a Campbell Scientific CSAT-3 sonic anemometer and a Licor-7500 CO_2/H_2O infrared gas analyzer positioned adjacent to each other at the top of the tower. These two instruments measured velocity, temperature and gas concentrations for the estimation of sensible heat flux, evapotranspiration (ET) and CO_2 exchanges (Fc) with the standard eddy covariance method (e.g. Baldocchi 2003). Half hourly statistics were computed.

The two-dimensional footprint model of Detto et al. (2006), previously tested for this site, was used for interpreting eddy-correlation measurements in the context of the contributing land cover area. The combined use of the footprint model and the satellite images allowed us to interpret the eddy-correlation observed surface flux and distinguish the source area of each PFT and bare soil to the measured flux, using the methodology in Detto et al. (2006).

Complete details of these measurements and data processing are available at Detto et al. (2006), Montaldo, Albertson, and Mancini (2008), and Montaldo et al. (2020).

LAI was measured indirectly through a ceptometer (Accupar model PAR-80, Decagon Devices Inc., Washington USA), which measures the PAR in the 400–700 nm waveband, and estimates the LAI from these readings (details are given in the instruction manual edited by Decagon Devices Inc.). LAI measurements were performed mainly during the grass growth season (Montaldo, Albertson, and Mancini 2008). Finally, specific leaf areas (LAI divided by dry biomass) of predominant grass (= 0.01 m^2 gDM^{-1}) and woody vegetation (= 0.005 m^2 gDM^{-1}) species were measured directly (by weighing the dry biomass).

2.2.2. Remote sensing and data assimilation approach for the case study

A total of 176 images were acquired (126 from Landsat 8 and 50 from Sentinel 2, see Figure 2c) for the 2016–2020 period, from which NDVI was derived at a 30 m spatial resolution. Images from the Sentinel 2 radiometer were acquired at the L1C level and atmospherically corrected with the Sen2-Cor tool of the Sentinel Application Platform (SNAP), or directly at the L2A level (already corrected). For Landsat 8 the L1TP product was used (it is radiometrically calibrated and orthorectified using ground control points and a digital elevation model), and the dark object subtraction (DOS) method (Chavez 1996) was used for the atmospheric correction. The coefficients of (9) were estimated using simultaneous NDVI data from remote sensors and LAI observations in the field (a total of 24 simultaneous days) distinguishing grass and trees ($\beta_1 = -0.435$, $\beta_2 = 1.014$ and $\beta_3 = 0.4029$ for grass in the fall-winter period, $\beta_1 = -0.141$, $\beta_2 = 1.720$ and $\beta_3 = 1.674$ for grass in the spring-summer period, $\beta_1 = 0$, $\beta_2 = 5.392$, and $\beta_3 = 0.486$ for trees).

In this case study, the LSM time step was half an hour, VDM time step was one day, the assimilation time step of NDVI data was variable according to data availability ranging from 2 days to 20 days with an average of 7 days, and the time step of the $m_{a,g}^\zeta$ and $m_{a,t}^\zeta$ updating was 3 weeks for both grass and trees (Figure 1). In the EnKF, N_e was 100, which is a sufficiently large number for accurate predictions (Crow and Wood 2003; Reichle et al. 2002).

We assumed the measurement errors being with zero mean and a standard deviation of 0.025, for both grass and tree NDVI. We generated the ensembles of initial grass and tree LAI values of grass (LAI_g) and tree (LAI_t) from a Gaussian distribution with means of 0.5 and 5.5, intentionally different from the observations, and a standard deviation σ_{LAI} of 0.2 for both grass and tree LAI. At each time step we generated the ensembles of incoming solar radiation and PAR by multiplying the measured values by a normally distributed random variable with mean zero and a standard deviation equal to 10%. It should be noted that the errors of the initial model states and parameters were uncorrelated.

The proposed assimilation approach was tested comparing the EnOL, EnKF, and EnKFdc approaches for nine initial $m_{a,g}^\zeta$ and $m_{a,t}^\zeta$ ensembles at most, generated with nine different initial $\hat{m}_{a,g}$ and $\hat{m}_{a,t}$ values (with the same SD_{mag} and SD_{mat} = 5% of the initial value).

A spatially distributed version of the multiscale assimilation approach was also applied to the area around the tower for the case study, running the model and assimilating NDVI data for LAI predictions in each cell of the spatial domain (Figure 3a).

3. Results

The NDVI map of the 500 m × 500 m area around the tower, derived from the Landsat-8 data of a dry summer day (08/14/2017), captured the spatial heterogeneity of the Orroli field site, allowing the identification of cells with predominately bare soil (NDVI < 0.22) and tree cover (NDVI >0.4) components (Figure 3a). The 2-component system (bare soil and tree) evolved from the start of the rainy seasons (typically in autumn in Sardinia), when grass grew replacing bare soil, and reaching its maximum growth in spring. Indeed, the distribution peak of the NDVI frequency in the examined area, which was mainly unimodal (Figure 3b), moved from ≈ 0.35 on a dry summer day to ≈ 0.47 on an autumn day, and reached ≈ 0.65 on a spring day (Figure 3b). The NDVI time evolution of the 289 cells in the examined area marked the heterogeneity and seasonality of the field (Figure 3c), with contrasting summer (NDVI decreased up to 0.2 with a high spread of the data
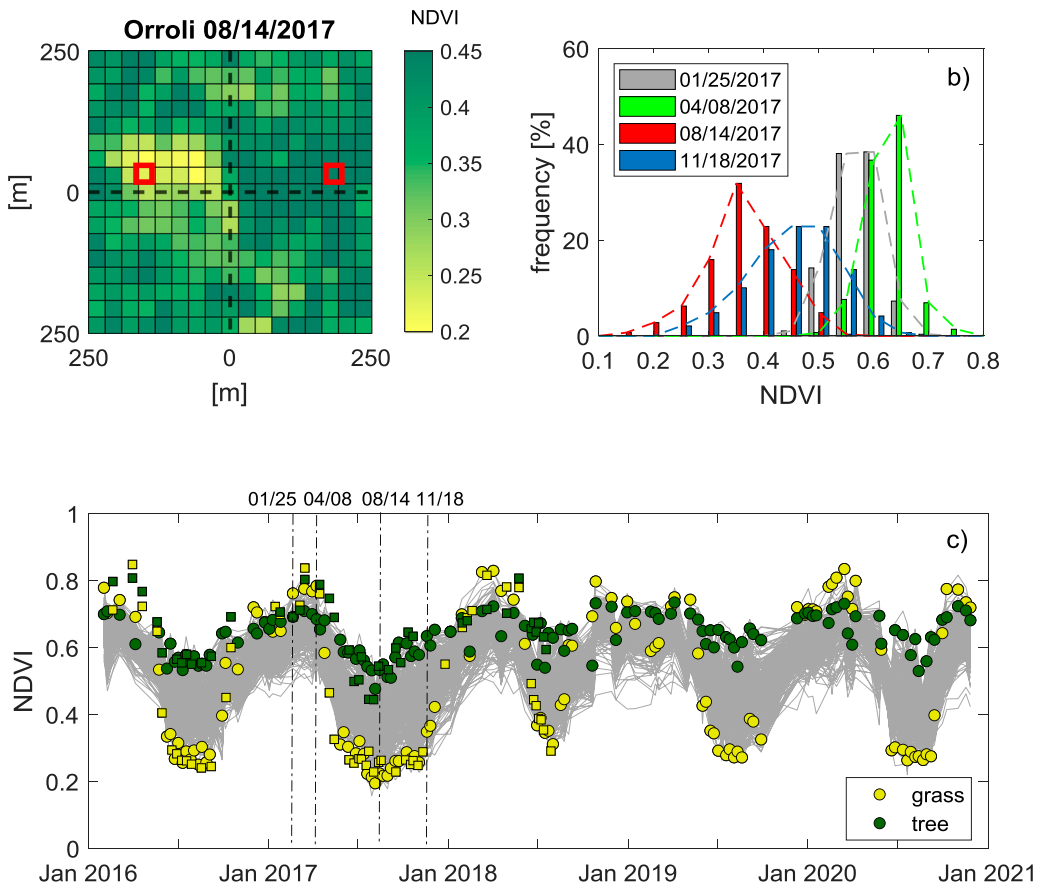

Figure 3. NDVI data of the field around the tower at the Sardinian site: a) the map in a dry day of the 2017 summer estimated from a Landsat 8 image (the selected representative grass and tree cells are market with edges in red; the tower is in the center of the map), b) frequency distributions during representative days of 2017 winter (01/25), spring (04/08), summer (08/14) and fall (11/18), c) evolution of the 289 cells in the field in time, yellow and green represent the selected representative cells of grass and tree respectively (circles: Landsat 8 data; squares: Sentinel 2 data).

distribution) and spring (NDVI up to 0.8 with a narrower distribution). Tree NDVI was much less variant over time than grass NDVI, which ranged from ≈ 0.2 (i.e. no grass, just bare soil) in summer to ≈ 0.75 in spring (Figure 3c). The use of the optical remote sensing data allowed to distinguish grass and tree cells. We selected the representative grass cell with low NDVI (≈ 0.2) and the representative tree cell with high NDVI (≈ 0.45) in the field from the NDVI map of the dry summer day (Figure 3a). We then used the NDVI time series of the two selected representative tree and grass cells (Figure 3c) for the data assimilation. In addition, for the spatially distributed application of EnKFdc, we assimilated the entire NDVI maps (Figure 3a), evaluating spatial patterns of the updated model parameters.

3.1. Data assimilation results

The coupled LSM-VDM were calibrated and validated in Montaldo, Albertson, and Mancini (2008) and Montaldo, Corona, and Albertson (2013) for this case study; the model parameters are given in Table 3. Here, the EnOL, EnKF and EnKFdc approaches are compared for increasing model uncertainties, evaluating the benefit of the assimilation approaches.

First, we tested the EnKF approach, generating $m_{a,g}^{\zeta}$ and $m_{a,t}^{\zeta}$ ensembles with slightly lower $\hat{m}_{a,g}$ and $\hat{m}_{a,t}$ values (= 0.02 d^{-1} and 0.0006 d^{-1}, respectively) than the calibrated values (= 0.032 d^{-1} and 0.001 d^{-1}, respectively) intentionally, assuming a moderate model error (Figure 4). The EnOL and EnKF approaches were compared for evaluating the performance of the filter in Figure 4, where the grass and tree LAI ensembles predicted using the EnOL and the EnKF approaches are plotted with the
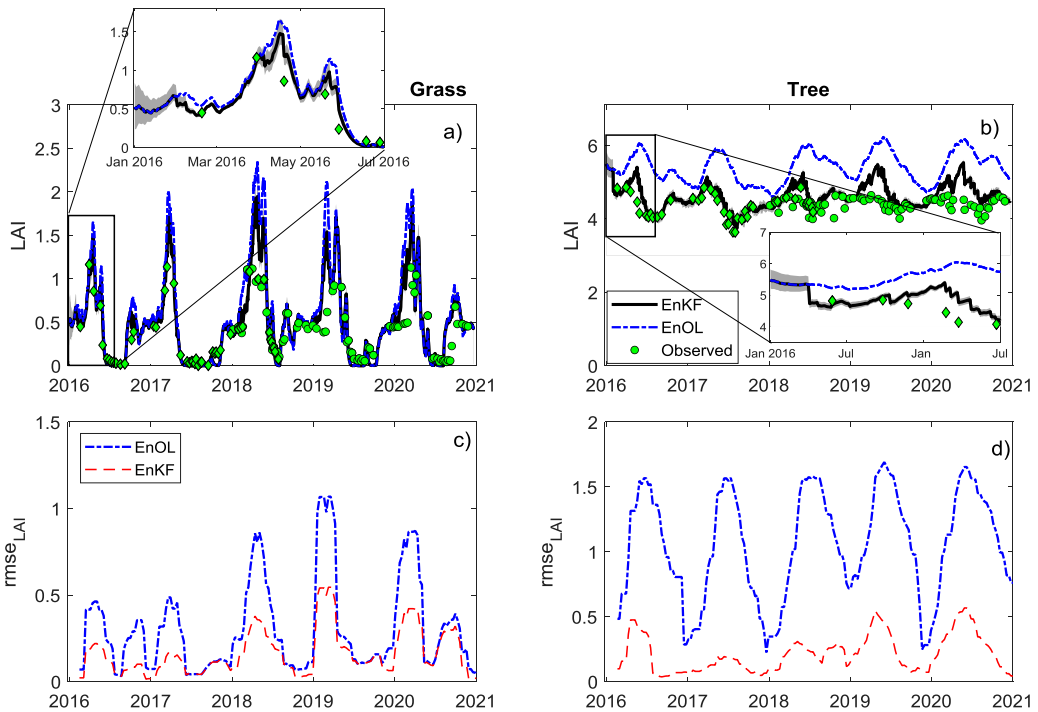

Figure 4. Assimilation results at the Sardinian site comparing the ensemble open loop configuration (EnOL) and the Ensemble Kalman filter (EnKF) approach for grass and tree LAI predictions for slightly low $\hat{m}_{a,g}$ (for grass) and $\hat{m}_{a,t}$ (for trees) values of 0.02 d^{-1} and 0.0006 d^{-1}: a) the ensemble mean grass LAI predictions using EnOL and EnKF and LAI observations derived by Landsat 8 and Sentinel 2 (obs.) (the 95% confidence interval of the EnKF LAI assimilation is shown as a gray band); c) the evolution of the rmse of the ensemble mean grass LAI predicted by EnOL and EnKF with respect to the observed LAI from remote data using a 60-day window, translated in 10-day increments; b) and c) are the same as a) and c), respectively, but for tree LAI.

LAI values derived by NDVI satellite observations using (9). The spread of the ensembles of grass and tree LAI^ζ decreased rapidly through time (Figure 4a and 4b). Compared to EnOL, the evolution of tree LAI with EnKF becomes closer to the observed tree LAI (Figure 3b). The EnKF guided $\overline{LAI}$ towards observations from the optical sensors (Figure 4), correcting the EnOL especially in spring and early-summer, mostly for the tree component (rmse of 0.26 for the whole period and = 0.40 for the springs using EnOL and rmse of 0.15 for the whole period and = 0.18 for the springs using EnKF for $\overline{LAI}$ of grass, and rmse of 4.01 using EnOL and rmse of 0.20 using EnKF for $\overline{LAI}$ of trees).

The performance of the EnKF assimilation scheme and the proposed EnKFdc were verified for increasing weak knowledge of the maintenance respiration coefficients. Generating $m_{a,g}^\zeta$ and $m_{a,t}^\zeta$ ensembles with initial $\hat{m}_{a,g}$ and $\hat{m}_{a,t}$ values (= 0.12 d^{-1} and 0.01 d^{-1}, respectively) being much higher than the calibrated values, meant that the persistent biases of the biomass balances were not removed by the EnKF-based assimilation approach (Figure 5a and 5c), and the EnKF assumption (mean zero of the model error) was not yet respected. Instead, the EnKFdc removed the bias in grass and tree LAI predictions through the dynamic updating of the $m_{a,g}^\zeta$ and $m_{a,t}^\zeta$ ensembles (Figure 6a and 6c). While using EnKF, the rmse of grass and tree $\overline{LAI}$ was still high (= 0.25 and 4.05, respectively, after one year), using the EnKFdc the rmse of the grass and tree $\overline{LAI}$ estimates decreased significantly (= 0.12 and 0.13, respectively, after one year). Indeed, in EnKFdc, the $m_{a,g}^\zeta$ and $m_{a,t}^\zeta$ ensembles decreased and converged close to the calibrated values after a learning (calibration) period (Figure 6a and 6c) because (24) guided the paths of the ensemble members toward
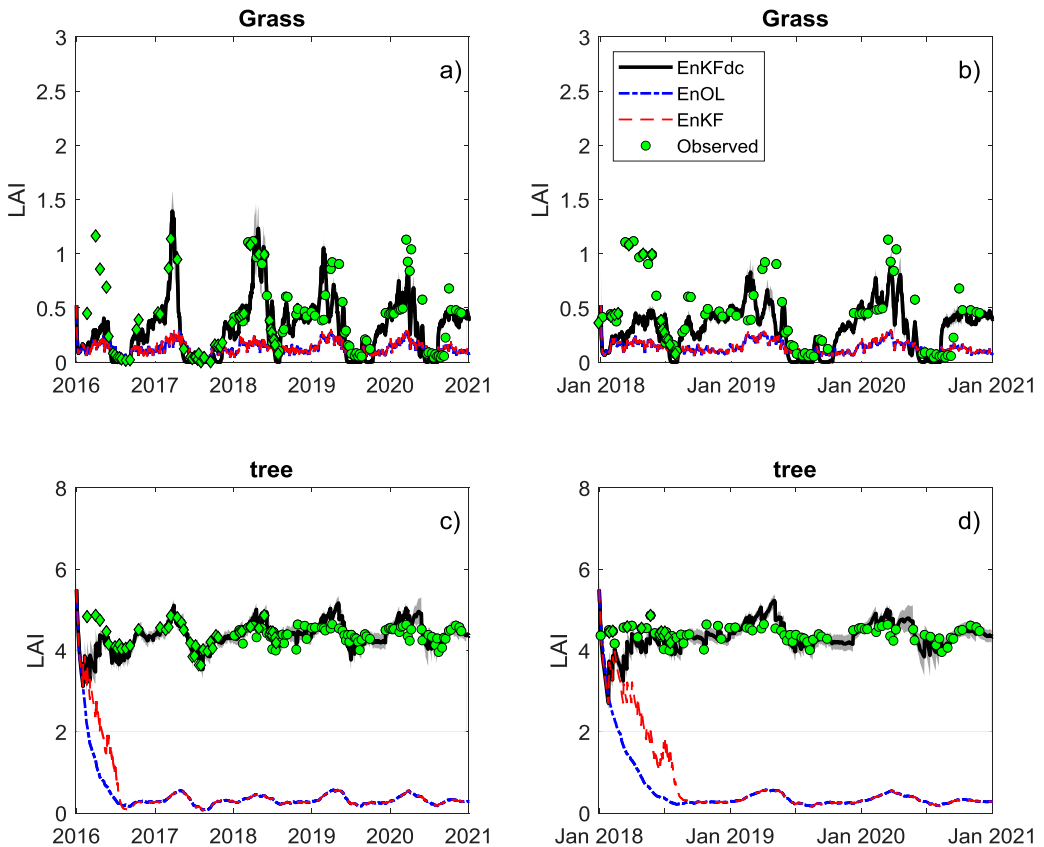

Figure 5. Assimilation results for grass and tree LAI predictions at the Sardinian site using initial high $\hat{m}_{a,g}$ (for grass) and $\hat{m}_{a,t}$ (for trees) values of 0.12 d^{-1} and 0.01 d^{-1}, respectively: a) and c) the comparison between LAI observations derived from assimilated remote optical data (obs.), the ensemble mean LAI predicted using the EnOL, EnKF, and EnKFdc approaches; b) and d) same of a) and b) but for a shorter time period.
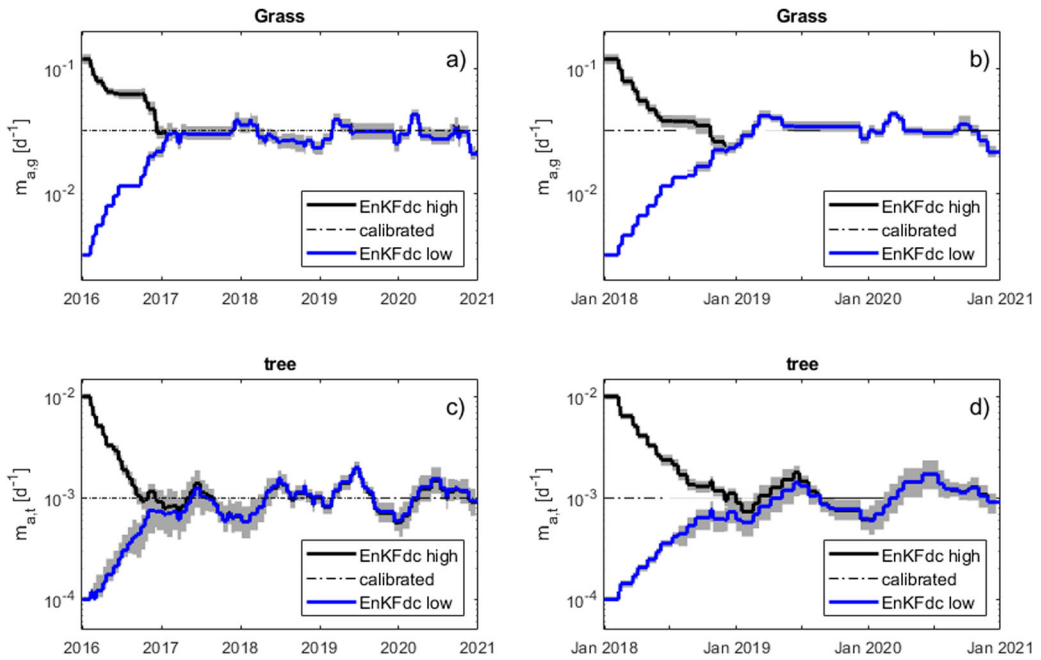
Figure 6. Assimilation results for grass and tree LAI predictions at the Sardinian site using initial high $\hat{m}_{a,g}$ (for grass) and $\hat{m}_{a,t}$ (for trees) values of 0.12 d^{-1} and 0.01 d^{-1}, respectively, and initial low $\hat{m}_{a,g}$ (for grass) and $\hat{m}_{a,t}$ (for trees) values of 0.0032 d^{-1} and 0.0001 d^{-1}, respectively: a) and c) the evolutions of the $m_{a,g}^{\zeta}$ and $m_{a,t}^{\zeta}$ ensembles using the EnKFdc approach (for reference, the calibrated values of m_{ag} and m_{at} are reported in dotted horizontal lines); b) and d) same of a) and b) but for a shorter time period.

the actual values (i.e. close to the calibrated values), and the assumption of the filter became satisfied.

We validated the EnKFdc assimilation scheme using a different start period, 1th January of 2018 instead of 1st January of 2016 (Figure 5b and 5d), always generating $m_{a,g}^{\zeta}$ and $m_{a,t}^{\zeta}$ ensembles with initial $\hat{m}_{a,g}$ and $\hat{m}_{a,t}$ values (= 0.12 d^{-1} and 0.01 d^{-1}, respectively) being much higher than the calibrated values (Figure 6b and 6d). Again, EnKFdc removed the bias in grass and tree LAI predictions and dynamically updated the $m_{a,g}^{\zeta}$ and $m_{a,t}^{\zeta}$ ensembles after one year (Figures 5 and 6).

In the same way, when initial $\hat{m}_{a,g}$ and $\hat{m}_{a,t}$ (= 0.0032 d^{-1} and 0.0001 d^{-1}, respectively) were largely lower than the calibrated values, the use of the proposed multi-scale assimilation approach allowed the increase of both $m_{a,g}^{\zeta}$ and $m_{a,t}^{\zeta}$ ensembles, which converged to values close to the calibrated values after one year (Figure 6).

We compared the performance of EnOL, EnKF and EnKFdc approaches for a large range of initial $\hat{m}_{a,g}$ (ranging from 0.0032 d^{-1} to 0.12 d^{-1}) and $\hat{m}_{a,t}$ (ranging from 0.0001 d^{-1} to 0.01 d^{-1}) (Figure 7). Using the EnOL approach, the *rmse* of the predicted grass $\overline{LAI}$ compared to the observed LAI derived by remote observations was very high (>0.5) for initial $\hat{m}_{a,g}$ lower than 0.02 d^{-1}, decreasing for $\hat{m}_{a,g}$ values close to the calibrated $m_{a,g}$, and increasing again for higher $\hat{m}_{a,g}$ up to a *rmse* of 0.35 (Figure 7a). When the EnKF approach was used, the *rmse* of the predicted grass $\overline{LAI}$ decreased but was lower than 0.3 only for initial $\hat{m}_{a,g}$ (= 0.015-0.045 d^{-1}), close to the calibrated value. Only the use of the proposed EnKFdc approach allowed the removal of model bias for all the range of initial $\hat{m}_{a,g}$, and the *rmse* of LAI always became lower than 0.15 (Figure 6a). Using EnOL, the *rmse* of the predicted tree $\overline{LAI}$ was even higher when compared to LAI observations, reaching a value close to 4.0 for the highest $\hat{m}_{a,t}$ (= 0.01 d^{-1}) and 2.6 for the lowest $\hat{m}_{a,t}$ (= 0.0001 d^{-1}, Figure 7b). Again, by only using EnKFdc, the model bias was removed for the whole range of initial $\hat{m}_{a,t}$
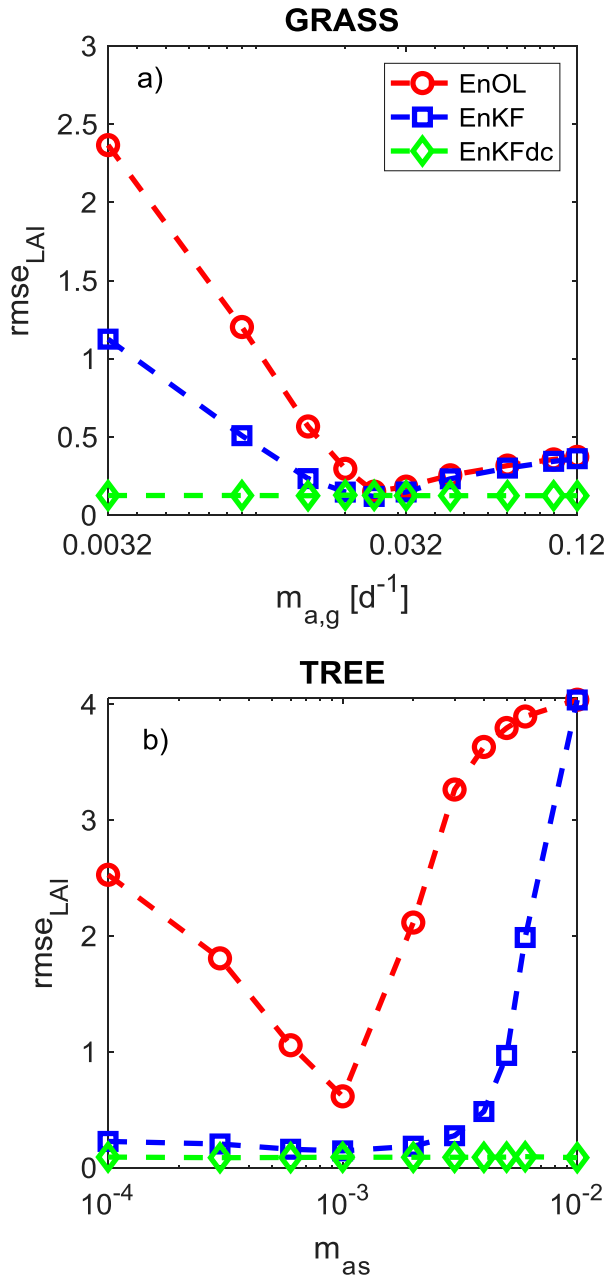
Figure 7. The rmse of ensemble mean LAI of a) grass and b) tree predicted using the EnOL, EnKF, and EnKFdc approaches with respect to the observed LAI derived from remote data, varying the initial $\hat{m}_{a,g}$ and $\hat{m}_{a,t}$ values.

with $rmse \approx 0.1$ (although EnKF performed sufficiently well, at least for the lowest $\hat{m}_{a,t}$ values with $rmse \approx 0.3$; see Figure 7b).

We also applied the proposed approach to the entire field around the tower (Figure 3a), running the spatially distributed version of EnKFdc from the 1th January of 2018, with still initial LAI values of grass and tree from a Gaussian distribution with means of 0.5 and 5.5, respectively, and still generating $m_{a,g}^{\zeta}$ and $m_{a,t}^{\zeta}$ ensembles with high initial $\hat{m}_{a,g}$ and $\hat{m}_{a,t}$ values (= 0.12 d^{-1} and 0.01 d^{-1}, respectively). While the predicted LAI (Figure 8a) were much higher than the estimated LAI
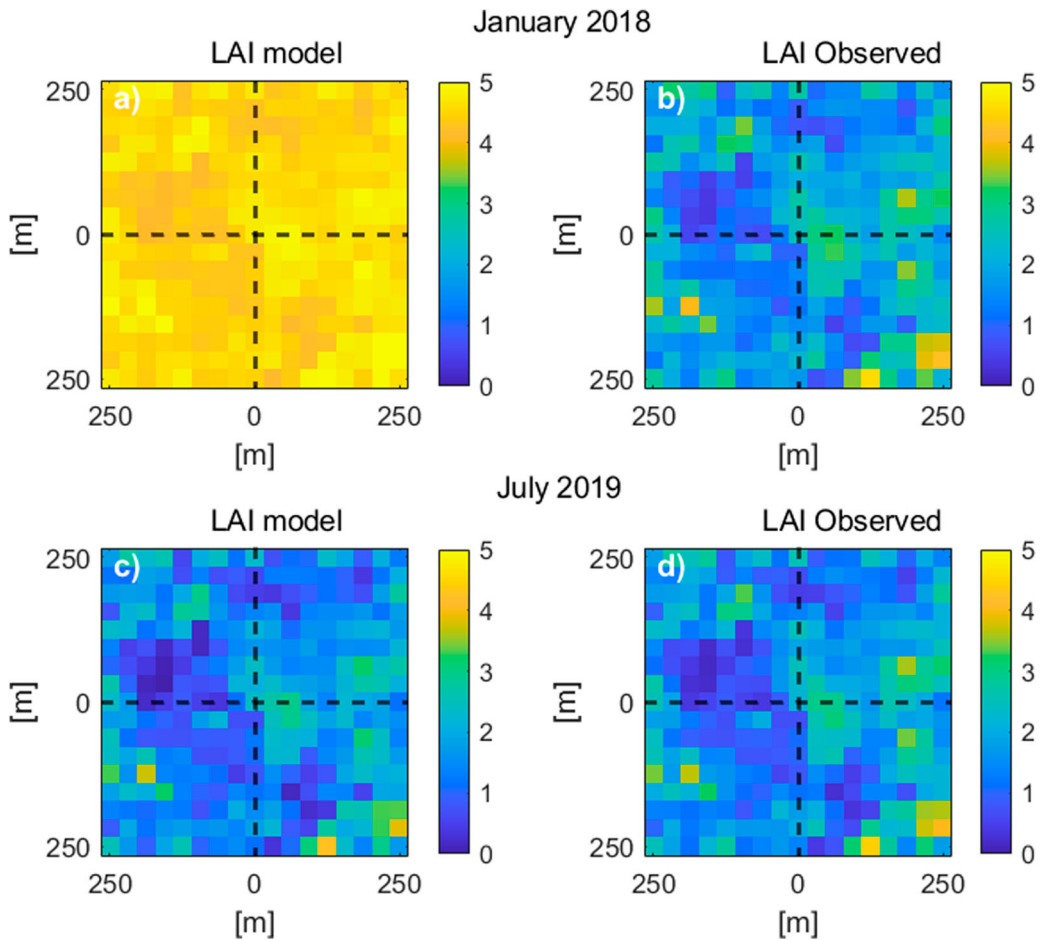
Figure 8. The LAI predictions for each cell of the field around the tower a) at the end of January 2018 and c) at the end of July 2019, compared with estimated LAI from remote sensor data b) at the end of January 2018 and d) at the end of July 2019.

from remote sensor observations (Figure 8b; mean predicted LAI of 4.56, mean observed LAI of 1.92) at the end of January 2018, the predictions of LAI (Figure 8c) became close to LAI observations (Figure 8d; mean predicted LAI of 1.60, mean observed LAI of 1.65) at the end of July 2019, because the EnKFdc removed model bias in all the cells of the spatial domain. Indeed, the difference between maintenance respiration coefficients of grass and trees and their calibrated values ($\Delta m_{a,g}$ and $\Delta m_{a,t}$, respectively) were high at the end of January 2018 (Figure 9a and 9b; mean $\Delta m_{a,g}$ of 0.05 and mean $\Delta m_{a,t}$ of 0.005), becoming negligible in July 2019 (Figure 9c and 9d; mean $\Delta m_{a,g}$ of 0.001 and mean $\Delta m_{a,t}$ of 0.0001.

4. Discussion

In heterogenous ecosystems, tree and grass covers and their spatial patterns are variable, depending on the water availability and incoming radiation (Sankaran et al. 2005); their vegetation mapping requires fine spatial and time resolutions of remote sensing data. In these ecosystems, the use of satellite images at coarser resolutions, like the widely used MODIS (Fox et al. 2018; Li et al. 2017) that provides optical data at 250 -500 m resolution, cannot provide adequate information for distinguishing grass and tree cover components, which are usually less than 50 m. The
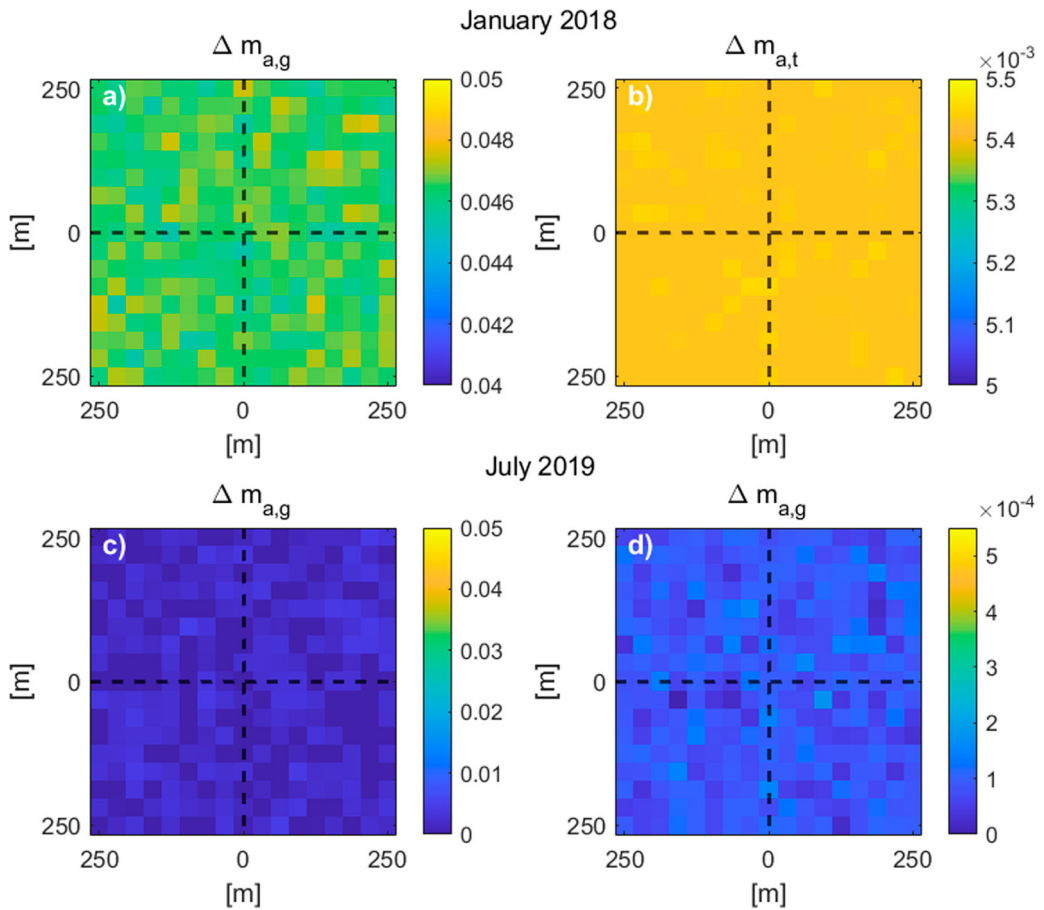
Figure 9. The difference between the maintenance respiration coefficients of a) grass and b) trees and their calibrated values ($\Delta m_{a,g}$ and $\Delta m_{a,t}$) for each cell in the field around the tower at the end of January 2018; c) and d) same as a) and b) at the end of July 2019.

combined use of the new satellites, Landsat 8 and Sentinel 2, whose data are freely available, is a promising solution, allowing monitoring of the Sardinian heterogenous ecosystem at fine temporal (average 7 days) and spatial (30 m) resolutions, including capturing the contrasting the seasonal dynamics of grass and trees. While few previous efforts of LAI data assimilation in LSM and VDM were concentrated on the use of MODIS (Demarty et al. 2007; Fox et al. 2018; Li et al. 2017; Ma et al. 2017; Migliavacca et al. 2009; Quaife et al. 2008), mainly due to the high time resolution (16 days) and the robustness of MODIS observations, we demonstrated that the Landsat 8 and Sentinel 2 NDVI data can be successfully used for data assimilation in heterogenous ecosystems. Coupling the observations of Landsat 8 and Sentinel 2, NDVI data became more frequent (average 7 days) and robust, starting in 2016.

Approaches have been developed to account for certain aspects of the spatial heterogeneity in ecohydrological models (Giorgi and Avissar 1997; Koster and Suarez 1992; Montaldo and Albertson 2003). The coupled LSM – VDM of Montaldo, Albertson, and Mancini (2008) follows the common mosaic of tiles approach, which divides the spatial domain of the model into a collection (or mosaic) of relatively homogenous land-surface elements (or 'tiles') and applies the model to each tile (Avissar and Pielke 1989; Koster et al. 2000; Koster and Suarez 1992). While previous efforts assimilated NDVI or LAI at the MODIS spatial scale (≥ 250 m) assuming the homogenous surface in grid cells

(Demarty et al. 2007; Li et al. 2017; Ma et al. 2017; Migliavacca et al. 2009;Quaife et al. 2008) are unable to distinguish grass and tree components, the proposed approach assimilated NDVI data of selected representative grass and tree cells of the heterogenous field in the coupled LSM-VDM, and successfully predicted grass and tree LAI.

The possibility to merge NDVI data and a VDM optimally for predicting accurately grass and tree LAI is demonstrated. The use of a typical Kalman filter, the ensemble Kalman filter (EnKF), as in previous efforts (Cheng et al. 2020; Huang et al. 2015; Kumar et al. 2019; Li et al. 2017; Ma et al. 2017; Migliavacca et al. 2009; Peng et al. 2021; Quaife et al. 2008; Tripathy et al. 2013), allowed the capture of LAI dynamics predicted by VDM, when moderate errors of key VDM parameters, like the m_a maintenance respiration coefficients of grass and tree components, were included (rmse = 0.15 and rmse = 0.2 respectively, Figure 4). Instead, poor estimates of m_a can bring to large VDM errors, and a main assumption of the Kalman filter (model error with zero-mean) was violated.

When the grass and tree m_a base values were weakly estimated (of one order of magnitude), and the parameter bias cannot be ignored compared to the random error, the EnKF approach (which assimilates NDVI data only) poorly predicted grass and tree LAI (rmse = 0.25 and rmse = 3.94 respectively, for high m_a base values). Instead, the proposed EnKFdc approach accepted the violation of the filter assumption in the early model runs, but removed the biased model error over time (rmse = 0.14 and rmse = 0.1 respectively, for high m_a base values), adjusting all the components of the $m_{a,g}^\zeta$ and $m_{a,t}^\zeta$ ensembles from the observed persistent bias in LAI (Figure 6). Previously, Montaldo, Albertson, and Mancini (2007) assimilated soil moisture observations in the same LSM using EnKF and developed an assimilation approach that dynamically calibrates a key soil water balance model parameter, the saturated hydraulic conductivity, as a function of the persistent bias in soil moisture predictions. This approach was useful when parameters largely differed from the calibrated values (Montaldo, Albertson, and Mancini 2007), and was applied by Montaldo et al. (2022) also assimilating Sentinel 1 radar data for soil moisture (Montaldo et al. 2022). Lü et al. (2011a; 2011b), Nie, Zhu, and Luo (2011) and Zhang et al. (2017) concentrated on assimilating soil moisture observed in the field using EnKF, and calibrating the few parameters in soil water balance models. We compared the performance of EnOL, EnKF and EnKFdc approaches for a large range of initial $\hat{m}_{a,g}$ (ranging from 0.0032 d^{-1} to 0.12 d^{-1}) and $\hat{m}_{a,t}$ (ranging from 0.0001 d^{-1} to 0.01 d^{-1}) (Figure 7), and wdemonstrated that the proposed dynamic calibration of key model parameters was also essential for assimilating NDVI data for LAI predictions. The proposed EnKFdc approach, which dynamically calibrates maintenance respiration coefficients of grass and trees, removed the bias in the biomass balance due to the bias in plant respiration (Figure 5), which was essential for balancing photosynthesis production, and reduced the model uncertainty (Figure 7). EnKFdc well corrected the VDM, guiding the entire ensemble of plant maintenance respiration coefficients toward the optimal value throughout the simulations. It should be noted that analogous solutions should be derivable for other VDMs, updating those parameters that highly impact model predictions. The new approach demonstrated its efficiency also when applied to the entire site around the tower (Figure 3a), which is characterized by a spatial variability of vegetation composition. The EnKFdc was able to guide the model for optimally updating the LAI of both vegetation components for all the cells in the field (the mean difference between the modeled and observed LAI in the field was only 3% in July 2019, Figure 8). Indeed, the maintenance respiration coefficients have been efficiently updated in all the cells of the field around the tower, with differences lower than 0.1% the calibrated values. We also demonstrated the effectiveness of the proposed assimilation method for evapotranspiration and CO_2 exchange predictions by comparing the predictions using the EnOL, EnKF, and EnKFdc approaches with ET and Fc observations of the eddy-correlation based tower. We evaluated the proposed assimilation approach for ET and Fc predictions using the full ranges of initial $\hat{m}_{a,g}$ and $\hat{m}_{a,t}$ values (Figure 10) and comparing the total predicted ET and Fc using the EnOL, EnKF, and EnKFdc approaches and the total observed ET and Fc (considering the days with observations only, which were 212 and 157 days, respectively). Using the
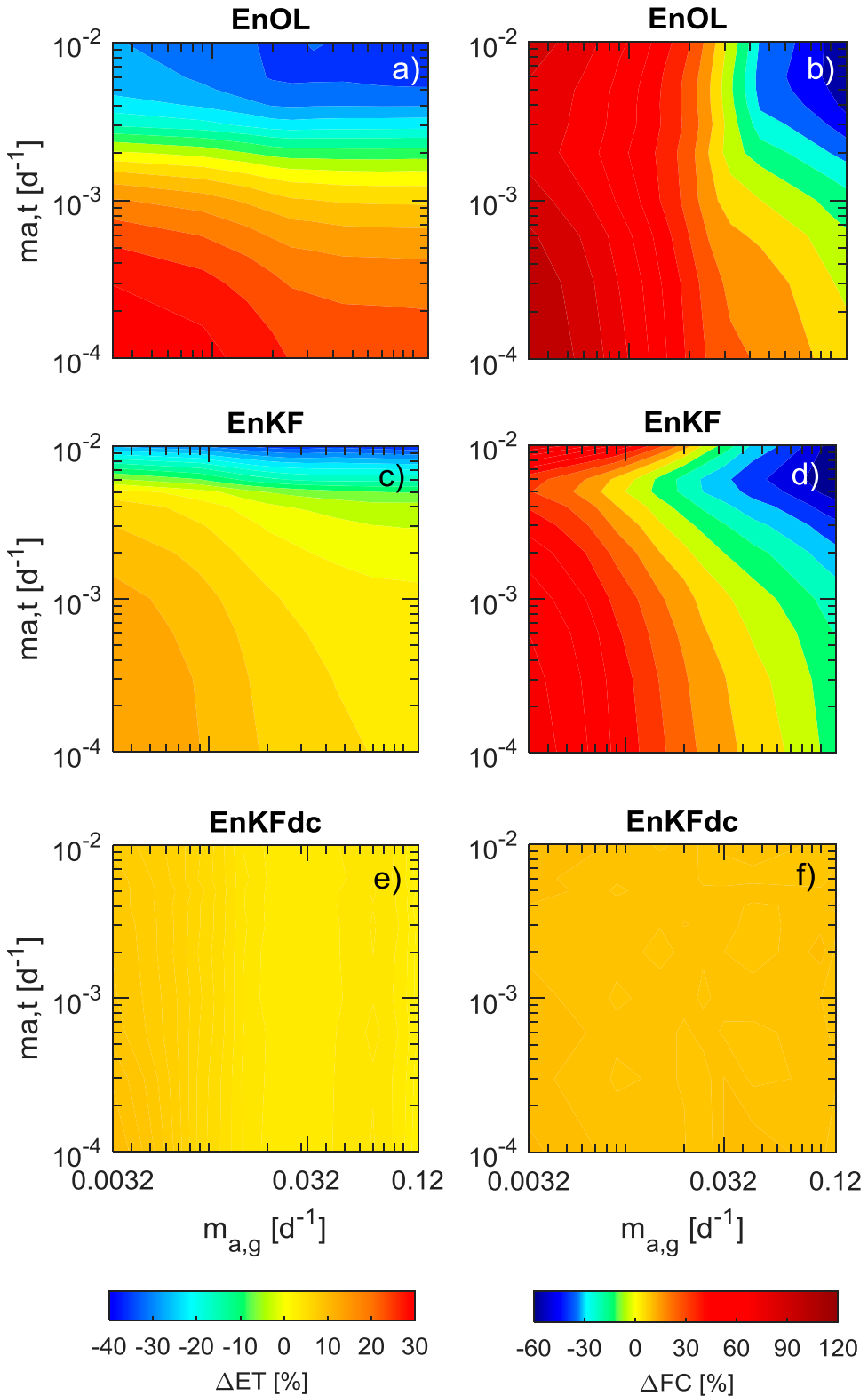
Figure 10. The comparison of the total evapotranspiration (ET, left panels) and carbon assimilation (Fc, right panels) predicted using the EnOL, EnKF, and EnKFdc approaches with the total observed ET and Fc varying the initial $\hat{m}_{a,g}$ and $\hat{m}_{a,t}$ values.

EnOL approach, the errors in grass and tree LAI predictions were reflected in ET predictions (Figure 10a). The EnKF approach was not enough for removing error bias in ET predictions, mainly for high $\hat{m}_{a,t}$ regardless of $\hat{m}_{a,g}$, under-estimating ET by up to 40–50%, and for low $\hat{m}_{a,g}$ (<0.02 d^{-1}) and $\hat{m}_{a,t}$ (< 0.003 d^{-1}) over-predicting ET by up to 15% (Figure 8c). The use of EnKFdc allowed the removal of model bias in ET predictions for the whole range of initial $\hat{m}_{a,g}$ and $\hat{m}_{a,t}$ values, remaining a slight over-prediction (up to 7%) only for extremely low initial $\hat{m}_{a,g} < 0.009$ d^{-1} (Figure 10e). Model bias in Fc predictions was even higher when the EnOL and EnKF approaches were used, with over-predictions up to 120% for low $\hat{m}_{a,g}$ and $\hat{m}_{a,t}$, and under-predictions up to 60% for high $\hat{m}_{a,g}$ and $\hat{m}_{a,t}$ (Figure 10b and 10d). The use of the proposed EnKFdc approach allowed correction of the model and Fc estimates were close to those observed, except the low mis-prediction of $\approx14\%$ for the highest (> 0.1 d^{-1}) and the lowest (< 0.009 d^{-1}) $\hat{m}_{a,g}$ (Figure 10f). Hence, for the robust prediction of two key terms of the land surface fluxes, the evapotranspiration and the CO_2 net flux, the EnKFdc approach is demonstrated to be essential. The proposed EnKFdc approach removed the model bias through a dynamic (on-line) calibration, allowing the correct prediction of ET and F_c for the entire range of the parameter values.

5. Conclusions

The assimilation of periodic observations of vegetation index, such as NDVI, from optical remote sensing platforms, allows for guiding the predictions of the coupled land surface model (LSM) and vegetation dynamic model (VDM) in heterogenous ecosystems. Indeed, the new Landsat 8 and Sentinel 2 optical sensors are available at such high temporal (≈ 7 days) and spatial (≈ 30 m) resolutions that they capture the dynamics of the main vegetation components (grass and trees). We demonstrated the possibility to successfully assimilate optical observations of grass and tree cover components of the Sardinian heterogenous ecosystem in a VDM for a long data series (5 years). We merged NDVI observations and the VDM optimally, to provide robust predictions of grass and tree LAI in the heterogenous ecosystem. Moreover, the inefficacy of a typical assimilation approach based on the Ensemble Kalman filter was demonstrated when a key VDM parameter, the m_a maintenance respiration coefficient, was estimated poorly, because it brings excessive model errors that alter the grass and tree biomass balances, and the Kalman filter assumption (model error with zero-mean) was violated.

Only using the proposed EnKFdc assimilation approach, the persistent bias of the model was removed through the adjusting of the model parameters ($m_{a,g}^{\zeta}$ and $m_{a,t}^{\zeta}$) ensembles related to the persistent bias in grass and tree LAI predictions.

Finally, we demonstrated that the proposed EnKFdc approach allowed good prediction of evapotranspiration and CO_2 exchanges, which are strictly related to LAI, when there was a strong, uncorrected estimate of the $\hat{m}_{a,g}$ and $\hat{m}_{a,t}$ base values. The proposed multiscale assimilation approach removed the model bias through a form of dynamic calibration.

The proposed assimilation approach can be useful in operational forecasting ecohydrological models over large domains, where the estimate of model parameters would be extremely uncertain.

Acknowledgements

Disclosure statement

Funding

Data availability statement

The data that support the findings of this study are available from the corresponding author upon reasonable request.

References

Albertson, J. D., and G. Kiely. 2001. "On the Structure of Soil Moisture Time Series in the Context of Land Surface Models." *Journal of Hydrology* 243 (1-2): 101–119. https://doi.org/10.1016/S0022-1694(00)00405-4.

Arora, V. 2002. "Modeling Vegetation as a Dynamic Component in Soil-Vegetation-Atmosphere Transfer Schemes and Hydrological Models." *Reviews of Geophysics* 40 (2): 2. https://doi.org/10.1029/2001RG000103.

Arora, V. K. 2003. "Simulating Energy and Carbon Fluxes Over Winter Wheat Using Coupled Land Surface and Terrestrial Ecosystem Models." *Agricultural and Forest Meteorology* 118 (1–2): 21–47. https://doi.org/10.1016/S0168-1923(03)00073-X.

Attarzadeh, R., and J. Amini. 2019. "Towards an Object-Based Multi-Scale Soil Moisture Product Using Coupled Sentinel-1 and Sentinel-2 Data." *Remote Sensing Letters* 10 (7): 619–628. https://doi.org/10.1080/2150704X.2019.1590872.

Attarzadeh, R., J. Amini, C. Notarnicola, and F. Greifeneder. 2018. "Synergetic Use of Sentinel-1 and Sentinel-2 Data for Soil Moisture Mapping at Plot Scale." *Remote Sensing* 10 (8): 18. https://doi.org/10.3390/rs10081285.

Avissar, R., and R. A. Pielke. 1989. "A Parameterization of Heterogeneous Land Surfaces for Atmospheric Numerical Models and its Impact on Regional Meteorology." *Monthly Weather Review* 117 (10): 2113–2136. https://doi.org/10.1175/1520-0493(1989)117<2113:APOHLS>2.0.CO;2.

Baldocchi, D. D. 2003. "Assessing the Eddy Covariance Technique for Evaluating Carbon Dioxide Exchange Rates of Ecosystems: Past, Present and Future." *Global Change Biology* 9 (4): 479–492. https://doi.org/10.1046/j.1365-2486.2003.00629.x.

Baldocchi, D. D., L. K. Xu, and N. Kiang. 2004. "How Plant Functional-Type, Weather, Seasonal Drought, and Soil Physical Properties Alter Water and Energy Fluxes of an oak-Grass Savanna and an Annual Grassland." *Agricultural and Forest Meteorology* 123 (1-2): 13–39. https://doi.org/10.1016/j.agrformet.2003.11.006.

Bonan, B., C. Albergel, Y. J. Zheng, A. L. Barbu, D. Fairbairn, S. Munier, and J. C. Calvet. 2020. "An Ensemble Square Root Filter for the Joint Assimilation of Surface Soil Moisture and Leaf Area Index Within the Land Data Assimilation System LDAS-Monde: Application Over the Euro-Mediterranean Region." *Hydrology and Earth System Sciences* 24 (1): 325–347. https://doi.org/10.5194/hess-24-325-2020.

Breshears, D. D. 2006. "The Grassland-Forest Continuum: Trends in Ecosystem Properties for Woody Plant Mosaics?" *Frontiers in Ecology and the Environment* 4 (2): 96–104. https://doi.org/10.1890/1540-9295(2006)004[0096:TGCTIE]2.0.CO;2.

Broge, N. H., and E. Leblanc. 2001. "Comparing Prediction Power and Stability of Broadband and Hyperspectral Vegetation Indices for Estimation of Green Leaf Area Index and Canopy Chlorophyll Density." *Remote Sensing of Environment* 76 (2): 156–172. https://doi.org/10.1016/S0034-4257(00)00197-8.

Brutsaert, W. 1982. "Evaporation into the Atmosphere." Kluwer Academic Publ., Dordrecht, Holland, 299 pp., 1982.

Cayrol, P., A. Chehbouni, L. Kergoat, G. Dedieu, P. Mordelet, and Y. Nouvellon. 2000. "Grassland Modeling and Monitoring with SPOT-4 VEGETATION Instrument During the 1997–1999 SALSA Experiment." *Agricultural and Forest Meteorology* 105 (1–3): 91–115. https://doi.org/10.1016/S0168-1923(00)00191-X.

Chavez, P. S. 1996. "Image-based Atmospheric Corrections Revisited and Improved." *Photogrammetric Engineering and Remote Sensing* 62 (9): 1025–1036.

Chen, L. J., L. Z. Wang, Y. Ma, and P. Liu. 2015. "Overview of Ecohydrological Models and Systems at the Watershed Scale." *Ieee Systems Journal* 9 (3): 1091–1099. https://doi.org/10.1109/JSYST.2013.2296979.

Cheng, Z. Q., J. H. Meng, J. L. Shang, J. G. Liu, J. X. Huang, Y. Y. Qiao, B. D. Qian, Q. Jing, T. F. Dong, and L. H. Yu. 2020. "Generating Time-Series LAI Estimates of Maize Using Combined Methods Based on Multispectral UAV Observations and WOFOST Model." *Sensors* 20 (21), https://doi.org/10.3390/s20216006.

Crow, W. T. 2003. "Correcting Land Surface Model Predictions for the Impact of Temporally Sparse Rainfall Rate Measurements Using an Ensemble Kalman Filter and Surface Brightness Temperature Observations." *Journal of Hydrometeorology* 4 (5): 960–973. https://doi.org/10.1175/1525-7541(2003)004<0960:CLSMPF>2.0.CO;2.

Crow, W. T., and E. F. Wood. 2003. "The Assimilation of Remotely Sensed Soil Brightness Temperature Imagery Into a Land Surface Model Using Ensemble Kalman Filtering: A Case Study Based on ESTAR Measurements During SGP97." *Advances in Water Resources* 26 (2): 137–149. https://doi.org/10.1016/S0309-1708(02)00088-X.

Demarty, J., F. Chevallier, A. D. Friend, N. Viovy, S. L. Piao, and P. Ciais. 2007. "Assimilation of Global MODIS Leaf Area Index Retrievals Within a Terrestrial Biosphere Model." *Geophysical Research Letters* 34 (15), https://doi.org/10.1029/2007GL030014.

Detto, M., N. Montaldo, J. D. Albertson, M. Mancini, and G. Katul. 2006. "Soil Moisture and Vegetation Controls on Evapotranspiration in a Heterogeneous Mediterranean Ecosystem on Sardinia, Italy." *Water Resources Research* 42 (8): 16. https://doi.org/10.1029/2005WR004693.

Dong, T. F., J. G. Liu, J. L. Shang, B. D. Qian, B. L. Ma, J. M. Kovacs, D. Walters, X. F. Jiao, X. Y. Geng, and Y. C. Shi. 2019. "Assessment of red-Edge Vegetation Indices for Crop Leaf Area Index Estimation." *Remote Sensing of Environment* 222: 133–143. https://doi.org/10.1016/j.rse.2018.12.032.

Dong, Y. Y., J. H. Wang, C. J. Li, G. J. Yang, Q. Wang, F. Liu, J. L. Zhao, H. F. Wang, and W. J. Huang. 2013. "Comparison and Analysis of Data Assimilation Algorithms for Predicting the Leaf Area Index of Crop Canopies." *Ieee Journal of Selected Topics in Applied Earth Observations and Remote Sensing* 6 (1): 188–201. https://doi.org/10.1109/JSTARS.2012.2208943.

Dunne, S., and D. Entekhabi. 2005. "An Ensemble-Based Reanalysis Approach to Land Data Assimilation." *Water Resources Research* 41 (2): 18. https://doi.org/10.1029/2004WR003449.

Eagleson, P. S. 2002. "Ecohydrology Darwinian Expression of Vegetation Form and Function." *Cambridge University Press*, New York, 443.

Evensen, G. 1994. "Sequential Data Assimilation with a Nonlinear Quasi-Geostrophic Model Using Monte-Carlo Methods to Forecast Error Statistics." *Journal of Geophysical Research-Oceans* 99 (C5): 10143–10162. https://doi.org/10.1029/94JC00572.

Evensen, G. 2003. "The Ensemble Kalman Filter: Theoretical Formulation and Practical Implementation." *Ocean Dynamics* 53 (4): 343–367. https://doi.org/10.1007/s10236-003-0036-9

Ewert, F. 2004. "Modelling Plant Responses to Elevated CO2: How Important is Leaf Area Index?" *Annals of Botany* 93 (6): 619–627. https://doi.org/10.1093/aob/mch101.

Famiglietti, J. S., and E. F. Wood. 1994. "Multiscale Modeling of Spatially-Variable Water and Energy-Balance Processes." *Water Resources Research* 30 (11): 3061–3078. https://doi.org/10.1029/94WR01498.

Fang, H. L., F. Baret, S. Plummer, and G. Schaepman-Strub. 2019. "An Overview of Global Leaf Area Index (LAI): Methods, Products, Validation, and Applications." *Reviews of Geophysics* 57 (3): 739–799. https://doi.org/10.1029/2018RG000608.

Fatichi, S., C. Pappas, and V. Y. Ivanov. 2016. "Modeling Plant-Water Interactions: An Ecohydrological Overview from the Cell to the Global Scale." *Wiley Interdisciplinary Reviews-Water* 3 (3): 327–368. https://doi.org/10.1002/wat2.1125.

Fernandez-Illescas, C. P., and I. Rodriguez-Iturbe. 2004. "The Impact of Interannual Rainfall Variability on the Spatial and Temporal Patterns of Vegetation in a Water-Limited Ecosystem." *Advances in Water Resources* 27 (1): 83–95. https://doi.org/10.1016/j.advwatres.2003.05.001.

Fernandez, J. B. G., M. R. G. Mora, and F. G. Novo. 2004. "Vegetation Dynamics of Mediterranean Shrublands in Former Cultural Landscape at Grazalema Mountains, South Spain." *Plant Ecology* 172 (1): 83–94. https://doi.org/10.1023/B:VEGE.0000026039.00969.7a

Fox, A. M., T. J. Hoar, J. L. Anderson, A. F. Arellano, W. K. Smith, M. E. Litvak, N. MacBean, D. S. Schimel, and D. J. P. Moore. 2018. "Evaluation of a Data Assimilation System for Land Surface Models Using CLM4.5." *Journal of Advances in Modeling Earth Systems* 10 (10): 2471–2494. https://doi.org/10.1029/2018MS001362.

Gao, F., J. Masek, M. Schwaller, and F. Hall. 2006. "On the Blending of the Landsat and MODIS Surface Reflectance: Predicting Daily Landsat Surface Reflectance." *Ieee Transactions on Geoscience and Remote Sensing* 44 (8): 2207–2218. https://doi.org/10.1109/TGRS.2006.872081.

Gim, H. J., C. H. Ho, S. Jeong, J. Kim, S. Feng, and M. J. Hayes. 2020. "Improved Mapping and Change Detection of the Start of the Crop Growing Season in the US Corn Belt from Long-Term AVHRR NDVI." *Agricultural and Forest Meteorology* 294. https://doi.org/10.1016/j.agrformet.2020.108143.

Giorgi, F., and R. Avissar. 1997. "Representation of Heterogeneity Effects in Earth System Modeling: Experience from Land Surface Modeling." *Reviews of Geophysics* 35 (4): 413–437. https://doi.org/10.1029/97RG01754.

Gupta, R. K., T. S. Prasad, and D. Vijayan. 2000. "Relationship Between LAI and NDVI for IRS LISS and LANDSAT TM Bands." *Remote Sensing for Land Surface Characterisation* 26 (7): 1047–1050. https://doi.org/10.1016/s0273-1177(99)01115-1.

Hanson, J. D., J. W. Skiles, and W. J. Parton. 1988. "A Multi-Species Model for Rangeland Plant Communities." *Ecological Modelling* 44 (1–2): 89–123. https://doi.org/10.1016/0304-3800(88)90084-1

Hill, T. C., T. Quaife, and M. Williams. 2011. "A Data Assimilation Method for Using low-Resolution Earth Observation Data in Heterogeneous Ecosystems." *Journal of Geophysical Research-Atmospheres* 116. https://doi.org/10.1029/2010jd015268.

Houborg, R., and M. F. McCabe. 2018. "Daily Retrieval of NDVI and LAI at 3 m Resolution via the Fusion of CubeSat, Landsat, and MODIS Data." *Remote Sensing* 10 (6), https://doi.org/10.3390/rs10060890.

Huang, C., Y. Chen, S. Q. Zhang, and J. P. Wu. 2018. "Detecting, Extracting, and Monitoring Surface Water from Space Using Optical Sensors: A Review." *Reviews of Geophysics* 56 (2): 333–360. https://doi.org/10.1029/2018RG000598.

Huang, J. X., L. Y. Tian, S. L. Liang, H. Y. Ma, I. Becker-Reshef, Y. B. Huang, W. Su, X. D. Zhang, D. H. Zhu, and W. B. Wu. 2015. "Improving Winter Wheat Yield Estimation by Assimilation of the Leaf Area Index from Landsat TM and MODIS Data Into the WOFOST Model." *Agricultural and Forest Meteorology* 204: 106–121. https://doi.org/10.1016/j.agrformet.2015.02.001.

Jarvis, P. G. 1976. "The Interpretation of the Variations in Leaf Water Potential and Stomatal Conductance Found in Canopies in the Field." *Philosophical Transactions of the Royal Society B* 273: 593–610.

Jasper, K., P. Calanca, D. Gyalistras, and J. Fuhrer. 2004. "Differential Impacts of Climate Change on the Hydrology of two Alpine River Basins." *Climate Research* 26 (2): 113–129. https://doi.org/10.3354/cr026113.

Jin, X. L., L. Kumar, Z. H. Li, H. K. Feng, X. G. Xu, G. J. Yang, and J. H. Wang. 2018. "A Review of Data Assimilation of Remote Sensing and Crop Models." *European Journal of Agronomy* 92: 141–152. https://doi.org/10.1016/j.eja.2017.11.002.

Koster, R. D., and M. J. Suarez. 1992. "Modeling the Land Surface Boundary in Climate Models as a Composite of Independent Vegetation Stands." *Journal of Geophysical Research-Atmospheres* 97 (D3): 2697–2715. https://doi.org/10.1029/91JD01696.

Koster, R. D., M. J. Suarez, A. Ducharne, M. Stieglitz, and P. Kumar. 2000. "A Catchment-Based Approach to Modeling Land Surface Processes in a General Circulation Model 1. Model Structure." *Journal of Geophysical Research-Atmospheres* 105 (D20): 24809–24822. https://doi.org/10.1029/2000JD900327.

Kross, A., R. Fernandes, J. Seaquist, and E. Beaubien. 2011. "The Effect of the Temporal Resolution of NDVI Data on Season Onset Dates and Trends Across Canadian Broadleaf Forests." *Remote Sensing of Environment* 115 (6): 1564–1575. https://doi.org/10.1016/j.rse.2011.02.015.

Kumar, S. V., D. M. Mocko, S. G. Wang, C. D. Peters-Lidard, and J. Borak. 2019. "Assimilation of Remotely Sensed Leaf Area Index Into the Noah-MP Land Surface Model: Impacts on Water and Carbon Fluxes and States Over the Continental United States." *Journal of Hydrometeorology* 20 (7): 1359–1377. https://doi.org/10.1175/JHM-D-18-0237.1.

Lambers, H., F. S. Chapin III, and T. L. Pons. 1998. "Plant Physiological Ecology." *Spinger-Verlag*, New York: 540.

Larcher, W. 1995. "Physiological Plant Ecology." *Springer*, 3rd edition: 506.

Li, X. J., F. J. Mao, H. Q. Du, G. M. Zhou, X. J. Xu, N. Han, S. B. Sun, G. L. Gao, and L. Chen. 2017. "Assimilating Leaf Area Index of Three Typical Types of Subtropical Forest in China from MODIS Time Series Data Based on the Integrated Ensemble Kalman Filter and PROSAIL Model." *Isprs Journal of Photogrammetry and Remote Sensing* 126: 68–78. https://doi.org/10.1016/j.isprsjprs.2017.02.002.

Ling, X. L., C. B. Fu, Z. L. Yang, and W. D. Guo. 2019. "Comparison of Different Sequential Assimilation Algorithms for Satellite-Derived Leaf Area Index Using the Data Assimilation Research Testbed (Version Lanai)." *Geoscientific Model Development* 12 (7): 3119–3133. https://doi.org/10.5194/gmd-12-3119-2019.

Lu, H. S., Z. B. Yu, R. Horton, Y. H. Zhu, Z. L. Wang, Z. C. Hao, and L. Xiang. 2011a. "Multi-scale Assimilation of Root Zone Soil Water Predictions." *Hydrological Processes* 25 (20): 3158–3172. https://doi.org/10.1002/hyp.8034.

Lu, H. S., Z. B. Yu, Y. H. Zhu, S. Drake, Z. C. Hao, and E. A. Sudicky. 2011b. "Dual State-Parameter Estimation of Root Zone Soil Moisture by Optimal Parameter Estimation and Extended Kalman Filter Data Assimilation." *Advances in Water Resources* 34 (3): 395–406. https://doi.org/10.1016/j.advwatres.2010.12.005.

Ma, R., L. Zhang, X. J. Tian, J. C. Zhang, W. P. Yuan, Y. Zheng, X. Zhao, and T. Kato. 2017. "Assimilation of Remotely-Sensed Leaf Area Index into a Dynamic Vegetation Model for Gross Primary Productivity Estimation." *Remote Sensing* 9 (3), https://doi.org/10.3390/rs9030188.

Margulis, S. A., D. McLaughlin, D. Entekhabi, and S. Dunne. 2002. "Land Data Assimilation and Estimation of Soil Moisture Using Measurements from the Southern Great Plains 1997 Field Experiment." *Water Resources Research* 38 (12): 18. https://doi.org/10.1029/2001WR001114.

McCabe, M. F., M. Rodell, D. E. Alsdorf, D. G. Miralles, R. Uijlenhoet, W. Wagner, A. Lucieer, et al. 2017. "The Future of Earth Observation in Hydrology." *Hydrolgy Earth System Science* 21 (7): 3879–3914. https://doi.org/10.5194/hess-21-3879-2017

Migliavacca, M., M. Meroni, L. Busetto, R. Colombo, T. Zenone, G. Matteucci, G. Manca, and G. Seufert. 2009. "Modeling Gross Primary Production of Agro-Forestry Ecosystems by Assimilation of Satellite-Derived Information in a Process-Based Model." *Sensors* 9 (2): 922–942. https://doi.org/10.3390/s90200922.

Montaldo, N., and J. D. Albertson. 2001. "On the use of the Force-Restore SVAT Model Formulation for Stratified Soils." *Journal of Hydrometeorology* 2 (6): 571–578. https://doi.org/10.1175/1525-7541(2001)002<0571:OTUOTF>2.0.CO;2.

Montaldo, N., and J. D. Albertson. 2003. "Multi-scale Assimilation of Surface Soil Moisture Data for Robust Root Zone Moisture Predictions." *Advances in Water Resources* 26 (1): 33–44. https://doi.org/10.1016/S0309-1708(02)00103-3.

Montaldo, N., J. D. Albertson, and M. Mancini. 2007. "Dynamic Calibration with an Ensemble Kalman Filter Based Data Assimilation Approach for Root-Zone Moisture Predictions." *Journal of Hydrometeorology* 8 (4): 910–921. https://doi.org/10.1175/JHM582.1.

Montaldo, N., J. D. Albertson, and M. Mancini. 2008. "Vegetation Dynamics and Soil Water Balance in a Water-Limited Mediterranean Ecosystem on Sardinia, Italy." *Hydrology and Earth System Sciences* 12 (6): 1257–1271. https://doi.org/10.5194/hess-12-1257-2008.

Montaldo, N., J. D. Albertson, M. Mancini, and G. Kiely. 2001. "Robust simulation of root zone soil moisture with assimilation of surface soil moisture data." *Water Resources Research* 37 (12): 2889–2900.

Montaldo, N., R. Corona, and J. D. Albertson. 2013. "On the Separate Effects of Soil and Land Cover on Mediterranean Ecohydrology: Two Contrasting Case Studies in Sardinia, Italy." *Water Resources Research* 49 (2): 1123–1136. https://doi.org/10.1029/2012WR012171.

Montaldo, N., M. Curreli, R. Corona, and R. Oren. 2020. "Fixed and Variable Components of Evapotranspiration in a Mediterranean Wild-Olive-Grass Landscape Mosaic." *Agricultural and Forest Meteorology* 280: 107769. https://doi.org/10.1016/j.agrformet.2019.107769.

Montaldo, N., A. Gaspa, and R. Corona. 2022. "Multiscale Assimilation of Sentinel and Landsat Data for Soil Moisture and Leaf Area Index Predictions Using an Ensemble-Kalman-Filter-Based Assimilation Approach in a Heterogeneous Ecosystem." *Remote Sensing* 14 (14).

Montaldo, N., R. Rondena, J. D. Albertson, and M. Mancini. 2005. "Parsimonious Modeling of Vegetation Dynamics for Ecohydrologic Studies of Water-Limited Ecosystems." *Water Resources Research* 41 (10), https://doi.org/10.1029/2005WR004094.

Montaldo, N., V. Toninelli, J. D. Albertson, M. Mancini, and P. A. Troch. 2003. "The Effect of Background Hydrometeorological Conditions on the Sensitivity of Evapotranspiration to Model Parameters: Analysis with Measurements from an Italian Alpine Catchment." *Hydrology and Earth System Sciences* 7 (6): 848–861. https://doi.org/10.5194/hess-7-848-2003.

Moore, G. W., and J. L. Heilman. 2011. "Proposed Principles Governing how Vegetation Changes Affect Transpiration." *Ecohydrology* 4 (3): 351–358. https://doi.org/10.1002/eco.232.

Ngadze, F., K. S. Mpakairi, B. Kavhu, H. Ndaimani, and M. S. Maremba. 2020. "Exploring the Utility of Sentinel-2 MSI and Landsat 8 OLI in Burned Area Mapping for a Heterogenous Savannah Landscape." *Plos One* 15 (5), https://doi.org/10.1371/journal.pone.0232962.

Nie, S., J. Zhu, and Y. Luo. 2011. "Simultaneous Estimation of Land Surface Scheme States and Parameters Using the Ensemble Kalman Filter: Identical Twin Experiments." *Hydrology and Earth System Sciences* 15 (8): 2437–2457. https://doi.org/10.5194/hess-15-2437-2011.

Noilhan, J., and S. Planton. 1989. "A Simple Parameterization of Land Surface Processes for Meteorological Models." *Monthly Weather Review* 117 (3): 536–549. https://doi.org/10.1175/1520-0493(1989)117<0536:ASPOLS>2.0.CO;2

Nouvellon, Y., S. Rambal, D. Lo Seen, M. S. Moran, J. P. Lhomme, A. Begue, A. G. Chehbouni, and Y. Kerr. 2000. "Modelling of Daily Fluxes of Water and Carbon from Shortgrass Steppes." *Agricultural and Forest Meteorology* 100 (2–3): 137–153. https://doi.org/10.1016/S0168-1923(99)00140-9.

Novick, K. A., P. C. Stoy, G. G. Katul, D. S. Ellsworth, M. B. S. Siqueira, J. Juang, and R. Oren. 2004. "Carbon Dioxide and Water Vapor Exchange in a Warm Temperate Grassland." *Oecologia* 138 (2): 259–274. https://doi.org/10.1007/s00442-003-1388-z.

Olsoy, P. J., J. Mitchell, N. F. Glenn, and A. N. Flores. 2017. "Assessing a Multi-Platform Data Fusion Technique in Capturing Spatiotemporal Dynamics of Heterogeneous Dryland Ecosystems in Topographically Complex Terrain." *Remote Sensing* 9 (10), https://doi.org/10.3390/rs9100981.

Parker, G. G. 2020. "Tamm Review: Leaf Area Index (LAI) is Both a Determinant and a Consequence of Important Processes in Vegetation Canopies." *Forest Ecology and Management* 477. https://doi.org/10.1016/j.foreco.2020.118496.

Peng, X. S., W. T. Han, J. Y. Ao, and Y. Wang. 2021. "Assimilation of LAI Derived from UAV Multispectral Data Into the SAFY Model to Estimate Maize Yield." *Remote Sensing* 13 (6), https://doi.org/10.3390/rs13061094.

Pettorelli, N., W. F. Laurance, T. G. O'Brien, M. Wegmann, H. Nagendra, and W. Turner. 2014. "Satellite Remote Sensing for Applied Ecologists: Opportunities and Challenges." *Journal of Applied Ecology* 51 (4): 839–848. https://doi.org/10.1111/1365-2664.12261.

Philip, J. R. 1957. "The Theory of Infiltration: 1. The Infiltration Equation and its Solution." *Soil Science* 83 (5): 345–358. https://doi.org/10.1097/00010694-195705000-00002

Porporato, A., and I. Rodriguez-Iturbe. 2002. "Ecohydrology - a Challenging Multidisciplinary Research Perspective." *Hydrological Sciences Journal-Journal Des Sciences Hydrologiques* 47 (5): 811–821. https://doi.org/10.1080/02626660209492985.

Potithep, S., N. K. Nasahara, H. Muraoka, S. Nagai, and R. Suzuki. 2010. "What is the Actual Relationship between LAI and VI in a Deciduous Broadleaf Forest?" *Networking the World with Remote Sensing* 38: 609–614.

Quaife, T., P. Lewis, M. De Kauwe, M. Williams, B. E. Law, M. Disney, and P. Bowyer. 2008. "Assimilating Canopy Reflectance Data Into an Ecosystem Model with an Ensemble Kalman Filter." *Remote Sensing of Environment* 112 (4): 1347–1364. https://doi.org/10.1016/j.rse.2007.05.020.

Ramirez-Sanz, L., M. A. Casado, J. M. de Miguel, I. Castro, M. Costa, and F. D. Pineda. 2000. "Floristic Relationship Between Scrubland and Grassland Patches in the Mediterranean Landscape of the Iberian Peninsula." *Plant Ecology* 149 (1): 63–70. https://doi.org/10.1023/A:1009846605935.

Reichle, R. H., G. J. M. De Lannoy, Q. Liu, R. D. Koster, J. S. Kimball, W. T. Crow, J. V. Ardizzone, et al. 2017. "Global Assessment of the SMAP Level-4 Surface and Root-Zone Soil Moisture Product Using Assimilation Diagnostics." *Journal of Hydrometeorology* 18 (12): 3217–3237. https://doi.org/10.1175/JHM-D-17-0130.1.

Reichle, R. H., R. D. Koster, J. R. Dong, and A. A. Berg. 2004. "Global Soil Moisture from Satellite Observations, Land Surface Models, and Ground Data: Implications for Data Assimilation." *Journal of Hydrometeorology* 5 (3): 430–442. https://doi.org/10.1175/1525-7541(2004)005<0430:GSMFSO>2.0.CO;2.

Reichle, R. H., Q. Liu, R. D. Koster, W. Crow, G. J. M. De Lannoy, J. S. Kimball, J. V. Ardizzone, et al. 2019. "Version 4 of the SMAP Level-4 Soil Moisture Algorithm and Data Product." *Journal of Advances in Modeling Earth Systems* 11 (10): 3106–3130. https://doi.org/10.1029/2019MS001729.

Reichle, R. H., J. P. Walker, R. D. Koster, and P. R. Houser. 2002. "Extended Versus Ensemble Kalman Filtering for Land Data Assimilation." *Journal of Hydrometeorology* 3 (6): 728–740. https://doi.org/10.1175/1525-7541(2002)003<0728:EVEKFF>2.0.CO;2.

Rodriguez-Iturbe, I. 2000. "Ecohydrology: A Hydrologic Perspective of Climate-Soil-Vegetation Dynamics." *Water Resources Research* 36 (1): 3–9. https://doi.org/10.1029/1999WR900210.

Ruehr, N. K., and N. Buchmann. 2010. "Soil Respiration Fluxes in a Temperate Mixed Forest: Seasonality and Temperature Sensitivities Differ among Microbial and Root-Rhizosphere Respiration." *Tree Physiology* 30 (2): 165–176. https://doi.org/10.1093/treephys/tpp106.

Sankaran, M., N. P. Hanan, R. J. Scholes, J. Ratnam, D. J. Augustine, B. S. Cade, J. Gignoux, et al. 2005. "Determinants of Woody Cover in African Savannas." *Nature* 438 (7069): 846–849. https://doi.org/10.1038/nature04070.

Scholes, R. J., and S. R. Archer. 1997. "Tree-grass Interactions in Savannas." *Annual Review of Ecology and Systematics* 28 (1): 517–544. https://doi.org/10.1146/annurev.ecolsys.28.1.517.

Scholze, M., M. Buchwitz, W. Dorigo, L. Guanter, and Q. G. Shaun. 2017. "Reviews and Syntheses: Systematic Earth Observations for use in Terrestrial Carbon Cycle Data Assimilation Systems." *Biogeosciences* 14 (14): 3401–3429. https://doi.org/10.5194/bg-14-3401-2017.

Thayn, J. B., and K. P. Price. 2008. "Julian Dates and Introduced Temporal Error in Remote Sensing Vegetation Phenology Studies." *International Journal of Remote Sensing* 29 (20): 6045–6049. https://doi.org/10.1080/01431160802235829.

Tripathy, R., K. N. Chaudhari, J. Mukherjee, S. S. Ray, N. K. Patel, S. Panigrahy, and J. S. Parihar. 2013. "Forecasting Wheat Yield in Punjab State of India by Combining Crop Simulation Model WOFOST and Remotely Sensed Inputs." *Remote Sensing Letters* 4 (1): 19–28. https://doi.org/10.1080/2150704X.2012.683117.

Vanrheenen, N. T., A. W. Wood, R. N. Palmer, and D. P. Lettenmaier. 2004. "Potential Implications of PCM Climate Change Scenarios for Sacramento-San Joaquin River Basin Hydrology and Water Resources." *Climatic Change* 62 (1-3): 257–281. https://doi.org/10.1023/B:CLIM.0000013686.97342.55.

Verrelst, J., G. Camps-Valls, J. Munoz-Mari, J. P. Rivera, F. Veroustraete, Jgpw Clevers, and J. Moreno. 2015. "Optical Remote Sensing and the Retrieval of Terrestrial Vegetation bio-Geophysical Properties - A Review." *Isprs Journal of Photogrammetry and Remote Sensing* 108: 273–290. https://doi.org/10.1016/j.isprsjprs.2015.05.005.

Villegas, J. C., J. E. Espeleta, C. T. Morrison, D. D. Breshears, and T. E. Huxman. 2014. "Factoring in Canopy Cover Heterogeneity on Evapotranspiration Partitioning: Beyond big-Leaf Surface Homogeneity Assumptions." *Journal of Soil and Water Conservation* 69 (3): 78A–83A. https://doi.org/10.2489/jswc.69.3.78A.

Wang, Q., S. Adiku, J. Tenhunen, and A. Granier. 2005. "On the Relationship of NDVI with Leaf Area Index in a Deciduous Forest Site." *Remote Sensing of Environment* 94 (2): 244–255. https://doi.org/10.1016/j.rse.2004.10.006.

Wigmosta, M. S., L. W. Vail, and D. P. Lettenmaier. 1994. "A distributed hydrology-vegetation model for complex terrain." *Water Resour. Res.* 30: 1665–1679. https://doi.org/10.1029/94WR00436.

Wigneron, J. P., A. Olioso, J. C. Calvet, and P. Bertuzzi. 1999. "Estimating Root Zone Soil Moisture from Surface Soil Moisture Data and Soil-Vegetation-Atmosphere Transfer Modeling." *Water Resources Research* 35 (12): 3735–3745. https://doi.org/10.1029/1999WR900258.

Williams, C. A., and J. D. Albertson. 2004. "Soil Moisture Controls on Canopy-Scale Water and Carbon Fluxes in an African Savanna." *Water Resources Research* 40 (9), https://doi.org/10.1029/2004WR003208.

Wythers, K. R., P. B. Reich, and D. P. Turner. 2003. "Predicting Leaf Area Index from Scaling Principles: Corroboration and Consequences." *Tree Physiology* 23 (17): 1171–1179. https://doi.org/10.1093/treephys/23.17.1171.

Zhang, H. J., H. J. H. Franssen, X. J. Han, J. A. Vrugt, and H. Vereecken. 2017. "State and Parameter Estimation of two Land Surface Models Using the Ensemble Kalman Filter and the Particle Filter." *Hydrology and Earth System Sciences* 21 (9): 4927–4958. https://doi.org/10.5194/hess-21-4927-2017.

Zheng, G., and L. M. Moskal. 2009. "Retrieving Leaf Area Index (LAI) Using Remote Sensing: Theories, Methods and Sensors." *Sensors* 9 (4): 2719–2745. https://doi.org/10.3390/s90402719.